Systems/Circuits

Differential Contribution of the Retrotrapezoid Nucleus and C1 Neurons to Active Expiration and Arousal in Rats

George M.P.R. Souza, Ruth L. Stornetta, Daniel S. Stornetta, Stephen B.G. Abbott, and Patrice G. Guyenet

Department of Pharmacology, University of Virginia, Charlottesville, Virginia 29908

Collectively, the retrotrapezoid nucleus (RTN) and adjacent C1 neurons regulate breathing, circulation and the state of vigilance, but previous methods to manipulate the activity of these neurons have been insufficiently selective to parse out their relative roles. We hypothesize that RTN and C1 neurons regulate distinct aspects of breathing (e.g., frequency, amplitude, active expiration, sighing) and differ in their ability to produce arousal from sleep. Here we use optogenetics and a combination of viral vectors in adult male and female *Th*-Cre rats to transduce selectively RTN (Phox2b$^+$/*Nmb*$^+$) or C1 neurons (Phox2b$^+$/*Th*$^+$) with Channelrhodopsin-2. RTN photostimulation modestly increased the probability of arousal. RTN stimulation robustly increased breathing frequency and amplitude; it also triggered strong active expiration but not sighs. Consistent with these responses, RTN innervates the entire pontomedullary respiratory network, including expiratory premotor neurons in the caudal ventral respiratory group, but RTN has very limited projections to brainstem regions that regulate arousal (locus ceruleus, CGRP$^+$ parabrachial neurons). C1 neuron stimulation produced robust arousals and similar increases in breathing frequency and amplitude compared with RTN stimulation, but sighs were elicited and active expiration was absent. Unlike RTN, C1 neurons innervate the locus ceruleus, CGRP$^+$ processes within the parabrachial complex, and lack projections to caudal ventral respiratory group. In sum, stimulating C1 or RTN activates breathing robustly, but only RTN neuron stimulation produces active expiration, consistent with their role as central respiratory chemoreceptors. Conversely, C1 stimulation strongly stimulates ascending arousal systems and sighs, consistent with their postulated role in acute stress responses.

Key words: **active expiration; arousal; breathing; C1 neurons; chemoreceptor; retrotrapezoid nucleus**

Significance Statement

The C1 neurons and the retrotrapezoid nucleus (RTN) reside in the rostral ventrolateral medulla. Both regulate breathing and the cardiovascular system but in ways that are unclear because of technical limitations (anesthesia, nonselective neuronal actuators). Using optogenetics in unanesthetized rats, we found that selective stimulation of either RTN or C1 neurons activates breathing. However, only RTN triggers active expiration, presumably because RTN, unlike C1, has direct excitatory projections to abdominal premotor neurons. The arousal potential of the C1 neurons is far greater than that of the RTN, however, consistent with C1's projections to brainstem wake-promoting structures. In short, C1 neurons orchestrate cardiorespiratory and arousal responses to somatic stresses, whereas RTN selectively controls lung ventilation and arterial P_{CO_2} stability.

Introduction

The retrotrapezoid nucleus (RTN) was originally defined as a bilateral region of the medulla oblongata located under the facial motor nuclei (Smith et al., 1989; Guyenet et al., 2019). In rats and mice, the neurons of this region include a subset with a distinctive expression profile and CO_2/H^+ sensing function (Phox2b$^+$, *Vglut2*$^+$, *Nmb*$^+$, *TASK-2*$^+$, *GPR4*$^+$, *Th*$^-$, Chat$^-$) (Shi et al., 2017; Guyenet et al., 2019). We use the term RTN to refer exclusively to these neurons (Guyenet et al., 2019). RTN neurons intermingle with C1 neurons caudally and with A5 neurons rostrally (Stornetta et al., 2006; Guyenet et al., 2013). C1 and A5 neurons are catecholaminergic, express Phox2a/b, and therefore are as efficiently transduced as RTN neurons by lentiviral vectors engineered with a PRSx8 promoter (Hwang et al., 2001; Marina et al., 2010; Abbott et al., 2013). The transduction of catecholaminergic neurons remains a source of uncertainty regarding the role of the RTN in respiratory control because C1 neurons also

Received Apr. 28, 2020; revised Aug. 13, 2020; accepted Sep. 14, 2020.

Author contributions: G.M.P.R.S., R.L.S., S.B.G.A., and P.G.G. designed research; G.M.P.R.S., D.S.S., and S.B.G.A. performed research; G.M.P.R.S., R.L.S., and S.B.G.A. analyzed data; G.M.P.R.S., R.L.S., D.S.S, S.B.G.A., and P.G.G. wrote the paper.

This work was supported by National Institutes of Health Grants HL28785 and HL074011 to P.G.G. and R01HL148004 to S.B.G.A.

The authors declare no competing financial interests.

Correspondence should be addressed to Patrice G. Guyenet at pgg@virginia.edu.

https://doi.org/10.1523/JNEUROSCI.1006-20.2020

stimulate breathing and arousal from sleep (Abbott et al., 2013; Burke et al., 2014).

These reservations notwithstanding, the most probable function of RTN neurons is to maintain stable arterial P_{CO_2} by adjusting lung ventilation (Guyenet et al., 2019). Most agree that RTN neurons regulate breathing frequency and tidal volume, but opinions vary as to whether RTN drives active expiration, the rhythmic contractions of abdominal and intercostal muscles that enhance expiration when metabolic demand increases (Iscoe, 1998; Huckstepp et al., 2016; Del Negro et al., 2018). Some consider active expiration as the purview of the parafacial expiratory oscillator, a group of neurons considered separate from RTN that reside in an adjoining area called lateral parafacial nucleus (pF_L) (Huckstepp et al., 2015; Del Negro et al., 2018). The pF_L is proposed to be one of three coupled brainstem respiratory oscillators, and necessary for active expiration (Anderson and Ramirez, 2017; Del Negro et al., 2018). The theory that an expiratory oscillator resides in the pF_L has several limitations: cellular level electrophysiological evidence of an oscillating circuit in the pF_L of adult rodents is missing, the phenotype of the cognate neurons is unidentified, and the area defined as pF_L contains numerous RTN cell bodies and dendrites (Del Negro et al., 2018; Guyenet et al., 2019).

We hypothesize that RTN neurons regulate CO_2 excretion by driving every aspect of breathing, including active expiration. This hypothesis is supported by four observations. Combined RTN plus C1 (RTN/C1) stimulation produces what appears to be active expiration based on plethysmography evidence (Abbott et al., 2011; Guyenet et al., 2019). Activation of Phox2b-derived ventral medullary neurons (likely including RTN/C1) triggers a pre-inspiratory burst of activity in the L1 spinal root *in vitro* (Cregg et al., 2017). RTN/C1 inhibition eliminates active expiration in an arterially perfused preparation (Marina et al., 2010). Finally, RTN/C1 neurons innervate the region of the medulla oblongata that contains the bulbospinal expiratory premotor neurons (Abbott et al., 2011; Silva et al., 2016). This evidence was obtained primarily using the aforementioned PRSx8 promoter that drives transgene expression in both RTN neurons and nearby catecholaminergic neurons. Critically, EMG-based evidence that activating RTN selectively recruits abdominal expiratory muscles in conscious rodents is unavailable.

The objective of the present study was to identify the effects produced by selectively activating either the RTN or the C1 neurons on breathing (rate, tidal volume, active expiration, sighing) and arousal from sleep. We used a *Th*-Cre rat to preferentially express Channelrhodopsin-2 (ChR2) in the C1 neurons without RTN involvement. This rat also allowed selective expression of ChR2 in RTN neurons by combining injections of the lentivirus PRSx8-ChR2-mCherry (Abbott et al., 2009) with AAV_5-flex-taCasp3-TEVp (Yang et al., 2013), which leads to Cre-dependent cell ablation of C1 neurons in the injection site. Diaphragm and abdominal muscle EMGs were monitored to determine whether active expiration could be produced by RTN or C1 stimulation. Neuroanatomical projections from RTN and C1 to abdominal premotor neurons and brainstem arousal-structures were mapped.

Materials and Methods

Animals. All experiments were conducted in accordance with the National Institutes of Health's *Guide for the care and use of laboratory animals* and approved by the University of Virginia Animal Care and Use Committee. We used 25 adult *Th*-Cre rats (18 male and 7 female) with a targeted insertion of IRES-Cre immediately after the translational stop in the open reading frame of *Th* (Sprague Dawley background; SD-$TH^{tm1(IRES\text{-}Cre)Sage}$, TGRA8400; RRID:RGD_12905029), procured from Envigo RMS and maintained as Cre homozygous as recommended by the company. Rats weighed 250-300 g at the time of virus microinjections and 300-550 g at the time of experiments. Animals were housed at 23°C-24°C under a standard artificial 12 h light-dark cycle with water and food provided *ad libitum* (Souza et al., 2019).

Animal preparation. All surgical procedures were conducted under aseptic conditions, and body temperature was maintained at 37°C with a servo-controlled heating pad. The depth of anesthesia was judged by the lack of reflex in response to a firm tail pinch. For brain injections and EEG/EMG electrode implantation, rats were anesthetized with a mixture of ketamine (75 mg/kg), xylazine (5 mg/kg), and acepromazine (1 mg/kg, i.m.). Additional anesthetic was administered if required (25% of the original dose, i.m.). Brain injections were performed on a stereotaxic frame (David Kopf Instruments), with the bite bar set at 3.5 mm below the interaural line for a flat skull (Souza et al., 2019). In all rats, incisions were closed in two layers using absorbable sutures for internal closures, and steel clips and VetClose adhesive for skin. Antibiotic (ampicillin, 125 mg/kg, i.p.) and analgesic (ketoprofen, 3-5 mg/kg, s.c.) were administered every 24 h for 3 d following surgery (Souza et al., 2018, 2019).

To label abdominal premotor neurons in the caudal ventral respiratory group (cVRG), 6 rats were microinjected with the retrograde tracer cholera toxin subunit B (CTB, List Biologicals Laboratories) in the lower thoracic/lumbar spinal cord (T12-L3) where abdominal motor neurons are located (Miller, 1987; Road et al., 2013). Rats were anesthetized as described above, placed on the stereotaxic frame, and an incision at the level of the T12-L3 was performed using a scalpel and fine scissors. The dorsal surface of a vertebra was removed with rongeurs to access the spinal cord. Microinjections of CTB were placed bilateral as described below. Animals were allowed to recover for 1 week before perfusion and tissue collection.

Viral vectors. RTN and C1 neurons are $Phox2b^+$ and are efficiently transduced by lentiviral vectors containing the artificial Phox2 promoter, PRSx8. For target RTN neurons, we used a combined injection of lentiviral vector LVV-PRSx8-ChR2(H134R)-mCherry (Abbott et al., 2009) (final titer for injection: 1.5×10^{10} TU/ml; Salk Institute) with an $rAAV_5$-Flex-taCaspase3-Tevp (final titer for injection: 3.2×10^{12} virus molecules/ml; UNC GTC Vector Core). Microinjection of this mixture in the RTN leads to selective ablation of C1 because Cre is expressed in these cells; hence, any remaining neurons expressing ChR2-mcherry are predominantly RTN neurons. To selectively transfect C1 neurons, we microinjected a Cre-dependent vector, $rAAV_2$-eF1α-DIO-hChR2 (H134R)-eYFP (UNC Vector Core, final titer for injection: 4.2×10^{12} virus molecules/ml). To control for the effect of the light on brain tissue ($n = 6$), $rAAV_2$-eF1α-DIO-eYFP (UNC Vector Core, final titer for injection: 4.5×10^{12} virus molecules/ml) was microinjected into the RTN/C1 region of 6 *Th*-Cre rats.

Brain and spinal cord microinjections and optic fiber placement. Brainstem microinjections were performed under electrophysiological guidance obtained from the facial motor nucleus antidromic potential (Abbott et al., 2009; Souza et al., 2019). The microinjections were performed using a glass micropipette and a picopump (Picospritzer, Parker Hannifin). For RTN targeting, three microinjections (60 nl each, 200 µm apart) were placed on the left side of the brain, 2000 µm lateral to the midline, 200 µm below the ventral pole of the facial motor nucleus. The most caudal injection was placed 200 µm caudal to the caudal end of the facial nucleus. For C1 neuron targeting, three microinjections (60 nl each, 200 µm apart; left side of the brain) were placed 1800 µm lateral to the midline, at a depth 100 µm below the ventral pole of the facial motor nucleus. The most rostral microinjection was placed 200 µm caudal from the caudal pole of the facial nucleus. A custom-made optrode [200 µm optic fiber (0.39 NA) connected to a 230 µm ceramic ferrule, ThorLabs] was placed 500 µm above the middle injection site and attached to the skull using dental cement as previously described (Basting et al., 2015).

After the completion of physiological studies, we microinjected the retrograde tracer CTB (0.5%, w/v) in the lower thoracic/lumbar spinal cord (T12-L3) of 6 rats (3 cases with RTN labeled, 3 cases with C1

labeled) to identify caudal medullary bulbospinal neurons presumed to be expiratory premotor neurons that innervate abdominal motor neurons. CTB was microinjected bilaterally (60 nl each) 500 μm lateral to the midline and 1600-1800 μm ventral from the surface of the spinal cord.

EEG and neck, abdominal, and diaphragm EMG. Custom-made EEG and neck EMG electrodes were implanted during the same surgery as microinjections. Three stainless-steel jeweler screws (P1 Technologies) were implanted epidurally: two over the left and right parietal bone and one in the left frontal bone. PFA-insulated (coated diameter 0.006 inch) multistrand stainless-steel wire (A-M Systems) connected screws for EEG to Amphenol pins in a plastic head stage (P1 Technologies). Neck (EMG) electrodes were implanted in the neck muscle (Souza et al., 2019).

After the arousal protocols (described below), rats were reanesthetized with isoflurane (2.5% in 100% O_2), and bipolar multistrand PFA-insulated (coated diameter 0.009 inch) stainless-steel (A-M Systems) electrodes were placed in the external oblique abdominal muscle (ABD_{EMG}) and in the diaphragm (DIA_{EMG}). The wires were tunneled under the skin and placed between the shoulder blades attached to a socket (P1 Technologies). Analgesic (ketoprofen, 3-5 mg/kg, s.c.) and antibiotic (ampicillin,125 mg/kg, i.p.) were administered after surgery. Rats were allowed to recover for 3 d before experimentation.

Physiologic recordings and data acquisition. The arousal effects of RTN and C1 photostimulation were examined at least 1 month after injections of virus, and before implantation of ABD_{EMG} and DIA_{EMG}. All the experiments were performed between 9:00 A.M. and 4:00 P.M., at an ambient room temperature of 27°C-28°C. Rats were habituated to the experimental conditions for 2 d before recording as described previously (Souza et al., 2019). On the day of the recording, rats were briefly anesthetized with isoflurane (2.0% in room air for <3 min) to connect the fiber optic implant to commuting fiber attached to a DPSS laser (470 nm, 200 mW, Laser Glow Technologies) and the head stage or the electrodes for ABD_{EMG} and DIA_{EMG} to an amplifier (World Precision Instruments). Rats were then placed in an unrestrained whole-body plethysmography chamber (5 L, EMKA Technologies). Air supply (2.5 L/min) was regulated by mass flow controllers (Alicat Scientific) and custom software. Experiments were performed in normoxic normocapnic conditions ($F_IO_2 = 0.21$; $F_ICO_2 = 0.0$) unless noted otherwise.

The recordings began after at least 1 h of habituation, and respiratory flow was recorded with a differential pressure transducer (EMKA Technologies). The signal was filtered and amplified (0.1-100 Hz, ×500), and digitized at 1 kHz. Respiratory frequency (f_R, in breaths/min) and tidal volume (V_T, in ml·100 × g^{-1}) were derived from the flow signal in Spike 2 (version 8, Cambridge Electronic Design). V_T (area under the curve during inspiration) was calibrated by injecting 5 ml of dry air into the chamber with a syringe (Souza et al., 2019). Minute-ventilation (V_E), the product of $f_R \times V_T$, was expressed in ml·min·100 × g^{-1}. EEG and EMG (including ABD_{EMG} and DIA_{EMG}) signals were bandpass filtered (EEG: 0.1-100 Hz, EMG: 100-3000 Hz), amplified (×1000), and digitized at 1 kHz. Importantly, in all cases included in the analysis of active expiration, we observed robust ABD_{EMG} phase-locked to expiration during periods of hypercapnia ($F_ICO_2 = 0.09$), which ensures the correct placement of the electrodes.

Protocol to measure sleep survival probability. We designed an incrementing-decrementing laser stimulation pattern (details in Results) to produce an incremental and smooth increase in f_R and V_T in sleeping rats, rather than the abrupt changes produced by a square wave-shaped stimulation pattern used in previous studies (Abbott et al., 2013; Burke et al., 2015a). The ventilatory changes during this pattern of stimulation replicate the ventilatory changes expected during an acute hypercapnia challenge (Souza et al., 2019). The total stimulation period was 90 s (10 ms pulse, 10 mW) and consisted of incremental increases in frequency of stimulation at 1, 3, 6, 9, 12, 18, and 20 Hz over 30 s, then a 30 s period of 20 Hz, followed by decrementing frequencies to zero over 30 s. To generate multiple trials for sleep survival analyses, stimulation was conducted every 10 min over the course of 5-6 h of testing. To estimate the probability of spontaneous arousal, rats were tested as described above; however, the laser output was set to 0 mW for the duration of the day.

Protocol to measure active expiration. Once habituated to the plethysmography chamber, the ABD_{EMG} and DIA_{EMG} were recorded for a 15 min baseline period, and then RTN or C1 was photostimulated tonically (20 Hz, 10 ms pulse, 20 s, 10 mW) or intermittently (train of 3, 10 ms pulses at a frequency of 1.5 Hz), as in Burke et al. (2015b). After trials in normoxic normocapnia, rats were exposed to up to 20 min of hyperoxic hypercapnia ($F_IO_2 = 0.65$; $F_ICO_2 = 0.09$) and after a recovery period in room air, up to 20 min of hypoxia ($F_IO_2 = 0.12$; $F_ICO_2 = 0.0$) to perform RTN and C1 stimulation trials over a background of high chemoreceptor activity. Hyperoxic hypercapnia was used to minimize the effects of CO_2 mediated by the carotid bodies (Souza et al., 2018).

Data analysis. EEG, EMG, and breathing pattern were used to determine sleep–wake state (Souza et al., 2019). NREM sleep was identified by the presence of slow-wave EEG activity (δ, 1-4 Hz), low neck EMG activity, and a regular breathing pattern. REM sleep was characterized by stable theta rhythm (6-8 Hz), EMG atonia, and high breathing variability. Quiet wake was identified by the absence of slow-wave EEG activity, generalized EEG desynchronization, increased EMG activity, and increased breathing variability. EEG arousals were required to be >10 s in duration, and the latency of arousal was considered as the time between stimulation onset and the onset of EEG desynchronization. Stimulation trials were only included in the analysis if the trial was preceded by at least 20 s of NREM sleep. A minimum of 8 successful trials was required for a case to be included in the analysis. Data obtained from the latency of arousal during the stimulation and no-stimulation (spontaneous arousal) were plotted as cumulative probability curves (sleep probability curves). The sigh probability was analyzed in the same fashion.

ABD_{EMG} and DIA_{EMG} signals were rectified and smoothed (500 ms), and amplitude was normalized to the range of respiratory-related EMG activity during the hyperoxic hypercapnia condition (i.e., ABD_{EMG} and DIA_{EMG} amplitudes during CO_2 were considered 100%). Amplitudes were expressed as % relative to CO_2. For the ABD_{EMG}, this refers to the maximum value during expiration minus the maximum value during inspiration ($Max_{EXP} - Max_{INSP}$), which considers changes in tonic EMG activity related to arousal and postural changes. For DIA_{EMG}, the maximum value during inspiration was used for analysis as this muscle group exhibited less variation associated with posture and arousal state.

Histology. After the experiments, animals were deeply anesthetized and then perfused transcardially with 4% PFA. Brains were removed and postfixed in the same fixative for 12-16 h at 4°C. Brains were sectioned (30 μm; transverse plane) the next day on a vibratome (VT-1000S, Leica Biosystems), and brain slices were stored in cryoprotectant at −20°C (Basting et al., 2015; Souza et al., 2018).

Immunohistochemistry to identify projections of RTN and C1 neurons was performed on free-floating sections. All immunohistochemistry procedures were conducted at room temperature unless otherwise noted. A 1 in 6 series of sections were rinsed, then blocked in a 100 mM Tris-buffered solution of 10% horse serum, 0.1% Triton-X, and 150 mM sodium chloride, and incubated with primary antibodies for 1 h at room temperature and 4°C overnight. Sections were then rinsed and incubated with secondary antibodies for 60 min and rinsed again before mounting on slides. Slides were covered with ProLong Gold with DAPI anti-fade mounting medium (P36931, Thermo Fisher Scientific).

Primary antibodies used to detect mCherry (marking RTN neuronal processes) were rabbit anti-dsRed (1:1000, Takara Biosciences, catalog #632496, RRID:AB_10013483) and to identify C1 neuronal processes chicken anti-GFP (1:1000, Aves Labs, catalog #GFP-1020, RRID:AB_10000240). To identify bulbospinal neurons of the cVRG, we used antibodies against CTB (goat anti-CTB, 1:2000, List Biological, catalog #703, RRID:AB_10013220). For the CGRP neurons, we used goat anti-CGRP (1:500, Abcam, catalog #ab36001, RRID:AB_725807). To identify TH neurons in the cVRG and pontine regions, we used mouse anti-TH (1:1000, Sigma Millipore, catalog #T1299, RRID:AB_477560).

All secondaries were obtained from Jackson ImmunoResearch Laboratories, and used at 1:500 as follows: Cy3 AffiniPure Donkey Anti-Rabbit IgG (H + L) (catalog #711-165-152, RRID:AB_2307443) to reveal rabbit anti-dsRed; AlexaFluor-488 AffiniPure Donkey Anti-Chicken IgY (IgG) (H + L)(catalog #703-545-155, RRID:AB_2340375) to reveal

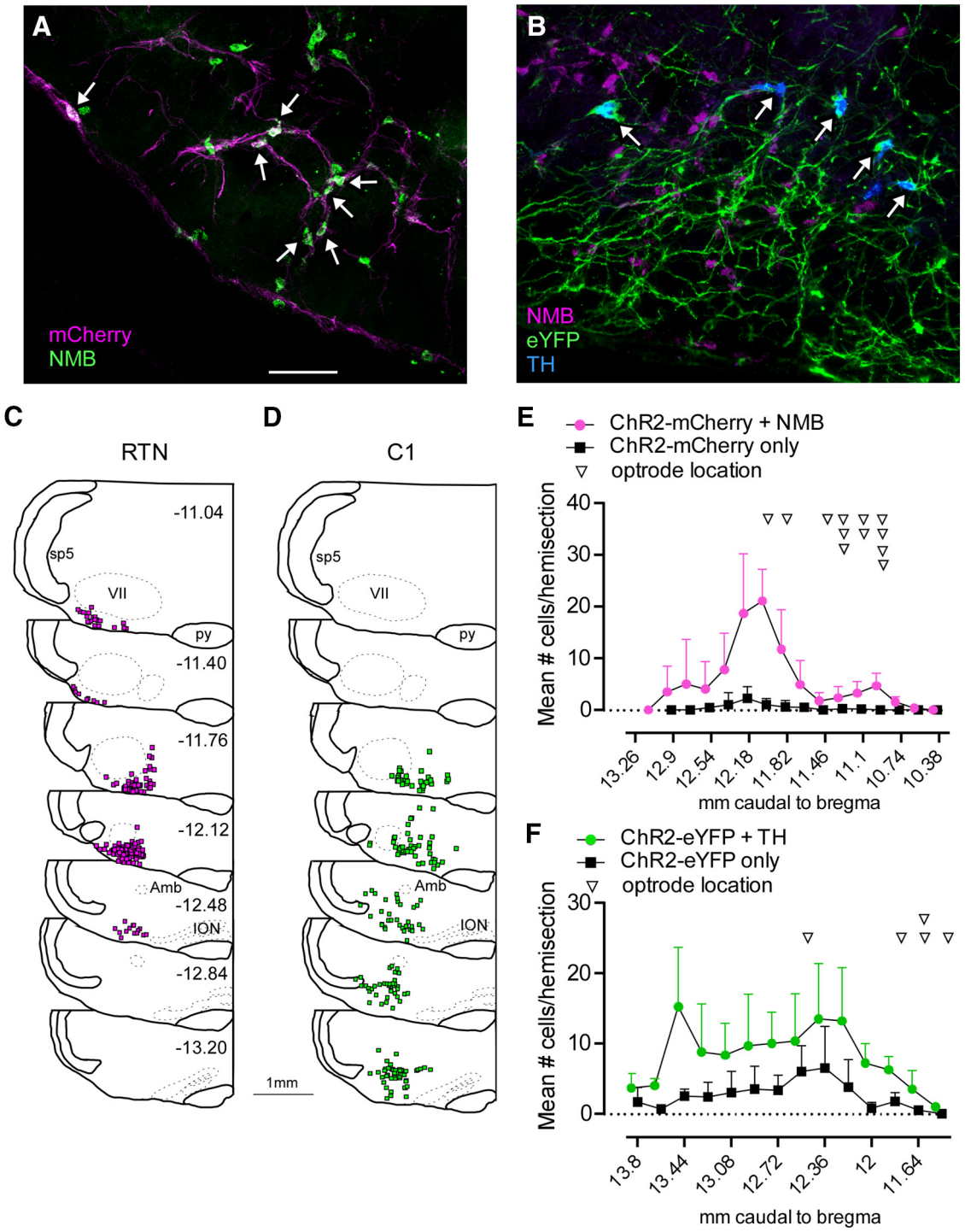

Figure 1. Selective expression of ChR2 in RTN and C1 neurons. ***A***, Combined ISH and immunohistochemistry showing selective transduction of RTN neurons (*Nmb*+mCherry, white arrows) in a *Th*-Cre rat in which *Th* neurons were ablated by injecting rAVV$_5$-Flex-taCaspase3-Tevp (transverse section; left). ***B***, ISH showing the selective transduction of C1 neurons (*Th*+eYFP, white arrows). ***C***, Rostral-to-caudal series of transverse sections (bregma levels in mm as indicated) depicting the location of *Nmb*+ChR2-mCherry-expressing neurons overlaid from 3 RTN-targeted cases. ***D***, Rostral-to-caudal series of transverse sections depicting the location of *Th*+ChR2-eYFP-expressing neurons overlaid from 3 C1-targeted cases. ***E***, Neuronal distribution and optical fiber location across bregma levels in RTN-targeted cases. ***F***, Neuronal distribution and optical fiber location across bregma levels in C1-targeted cases. References to mm caudal to bregma after Paxinos and Watson (2014). Scale bar, 100 μm.

chicken anti-GFP; AlexaFluor-647 AffiniPure Donkey Anti-Goat IgG (H + L)(catalog #705-605-147, RRID:AB_2340437) to reveal goat anti-CTB or goat-anti-CGRP; AlexaFluor-488 AffiniPure F(ab′)2 Fragment Donkey Anti-Mouse IgG (H + L)(catalog #715-546-150, RRID:AB_2340849), or Cy3 AffiniPure F(ab′)2 Fragment Donkey Anti-Mouse IgG (H + L)(catalog #715-166-150, RRID:AB_2340816) to reveal mouse anti-TH.

To establish selectivity, RTN neurons were identified by the presence of *Neuromedin B* mRNA (*Nmb*) in an area from ~400 μm caudal to the facial nucleus extending to the level of the exit of the facial nerve. According to Shi et al. (2017), Nmb is a more restrictive marker of RTN-chemosensitive neurons than Phox2b immunoreactivity. C1 neurons were identified by the presence of *Th* mRNA within a region extending from the split of the lateral reticular nucleus to 300 μm rostral to the

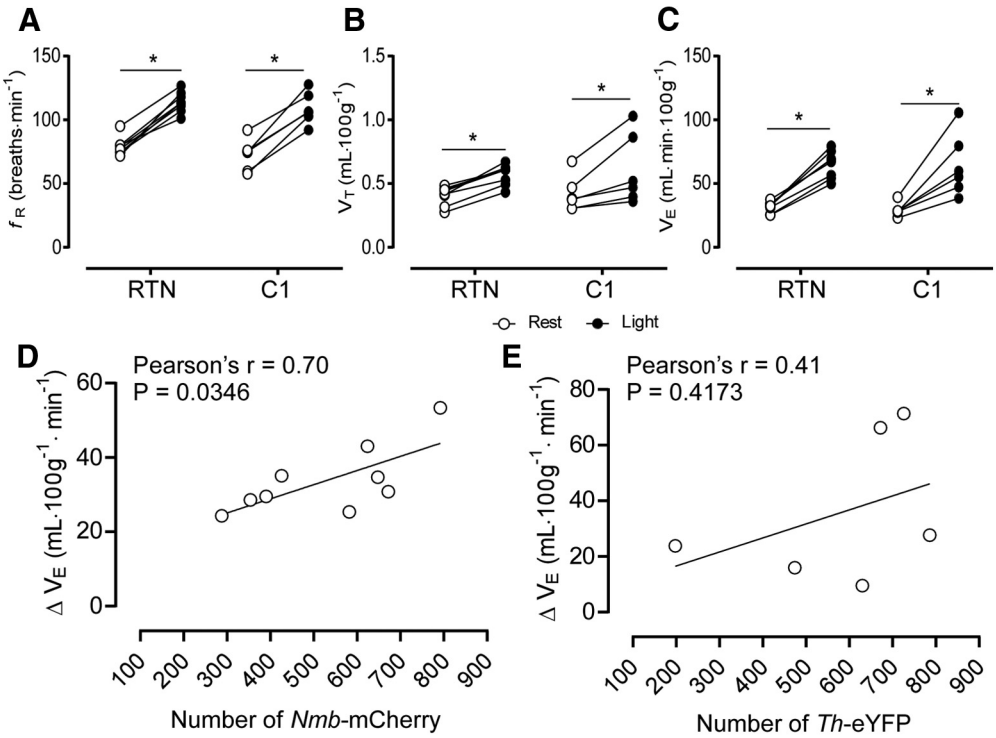

Figure 2. Selective stimulation of RTN or C1 neurons activates breathing to a comparable degree. ***A***, Changes in f_R produced by photostimulation of RTN or C1 neurons. Two-way ANOVA for repeated measures: interaction between cell type and stimulation, $F_{(1,12)} = 0.093$, $p = 0.764$; effect of cell type, $F_{(1,12)} = 1.40$, $p = 0.258$; effect of stimulation, $F_{(1,12)} = 216.9$, $p < 0.0001$. ***B***, Change in V_T produced by stimulation of RTN or C1 neurons. Two-way ANOVA for repeated measures: interaction between cell type and stimulation, $F_{(1,12)} = 0.18$, $p = 0.6754$; effect of cell type, $F_{(1,12)} = 0.086$, $p = 0.7732$; effect of stimulation, $F_{(1,12)} = 40.54$, $p < 0.0001$. ***C***, Changes in V_E produced by stimulation of RTN or C1 neurons. Two-way ANOVA for repeated measures: interaction between cell type and stimulation, $F_{(1,3)} = 0.093$, $p = 0.7799$; effect of cell type, $F_{(1,7)} = 0.052$, $p = 0.8252$; effect of stimulation, $F_{(1,7)} = 63.33$, $p < 0.0001$. ***D***, Correlation between number of RTN neurons (*Nmb*+ChR2-mCherry) and changes in V_E produced by photostimulation. ***E***, Correlation between number of C1 neurons (*Th*+ChR2-mCherry) and changes in V_E produced by photostimulation. *$p < 0.05$ (Bonferroni's multiple comparisons).

caudal pole of the facial motor nucleus. To identify Nmb and Th mRNA simultaneously, we used catalog probes for rat Th and Nmb (Rn-Th: 314651; Rn-Nmb: 494791) with multiplex *in situ* hybridization (ISH) using RNAscope (Advanced Cell Diagnostics) according to the manufacturer's directions. A 1 in 6 series of serial sections were briefly washed in sterile PBS, mounted on charged slides, and dried overnight. To identify *Nmb* and *Th* neurons expressing either ChR2-mCherry or ChR2-eYFP, we used immunohistochemistry performed on the slide after the RNAScope procedure with antibodies against mCherry or eYFP along with their respective secondaries as described above with a slight modification. Immediately following RNAScope, sections were rinsed and then incubated in blocking solution for 10 min followed by incubation in primary at room temperature for 60 min, rinsed and incubated in secondary for 30 min, and rinsed and then covered as described above.

Cells were mapped and counted in Neurolucida software (version 11, MBF Bioscience) using an AxioImager M2 (Carl Zeiss) after methods previously described (Stornetta et al., 2006). Digital photomicrographs were acquired with the same microscope in grayscale using a Hamamatsu C11440 Orca-Flash 4.0LT digital camera (MBF Bioscience). Filter settings for Cy3 or Atto 550, Alexa-488, and Atto 647 fluorophores were as follows: Alexa-488, excitation of 500 nm, emission of 535 nm; Atto 550 or Cy3, excitation of 545, emission of 605 nm; Atto 647, excitation of 640 nm, emission of 690 nm. Only cell profiles that included a nucleus in the plane of section were counted and/or mapped. Between 9 and 12 sections were counted per rat. Composite maps of ChR2-expressing RTN and C1 neurons reflect compiled maps of 3 individual cases for each group matched for rostrocaudal level, and resized in the *x-y* plane to fit an idealized drawing of the brain in coronal section based on the location of the pyramids, facial nucleus, and spinal trigeminal nerve tract. For presentation, images were pseudo-colored, brightness and contrast were optimized for visibility, all pixels in the image were adjusted equally, and these modifications were performed in Fiji software (Schindelin et al., 2012).

Experimental design and statistical analysis. Statistical comparisons were made using Prism software (version 8.4, GraphPad). Following either D'Agostino-Pearson or Shapiro-Wilk tests for normality, differences within and between groups were determined using repeated-measures two-way ANOVA with Bonferroni's post-test. Mann–Whitney test was used when data were not normally distributed. Pearson's correlation and least-squares linear regression were used to assess the correlation between the number of neurons expressing ChR2 and the ventilatory stimulation (ΔV_E) produced by photostimulation. All F and p values for the interaction effects and individual treatment effects are reported either in the text or in the corresponding figure legend. Degrees of freedom for each F value are designated by subscripts as per convention. Data are reported as mean ± SD, unless stated otherwise; and differences were considered significant when $p < 0.05$.

Results

Histologic evidence for selective targeting of ChR2 to RTN or C1 neurons

Five to 6 weeks after injecting a mixture of LVV-PRSx8-ChR2 (H134R)-mCherry and rAAV$_5$-Flex-taCaspase3-Tevp into the rostral ventrolateral medulla, mCherry-immunoreactive cell bodies were located below the facial motor nucleus on the injected (left) side, and most (93.7 ± 5.0%, range: 82%-100%, $n = 12$) contained *Nmb* mRNA (Fig. 1*A*,*C*,*E*). Based on previous work, these *Nmb*$^+$ cells are excitatory neurons that also express Phox2b, which we define as the RTN (Shi et al., 2017). This nucleus contains ~1100 such neurons per side in rats. Based on the

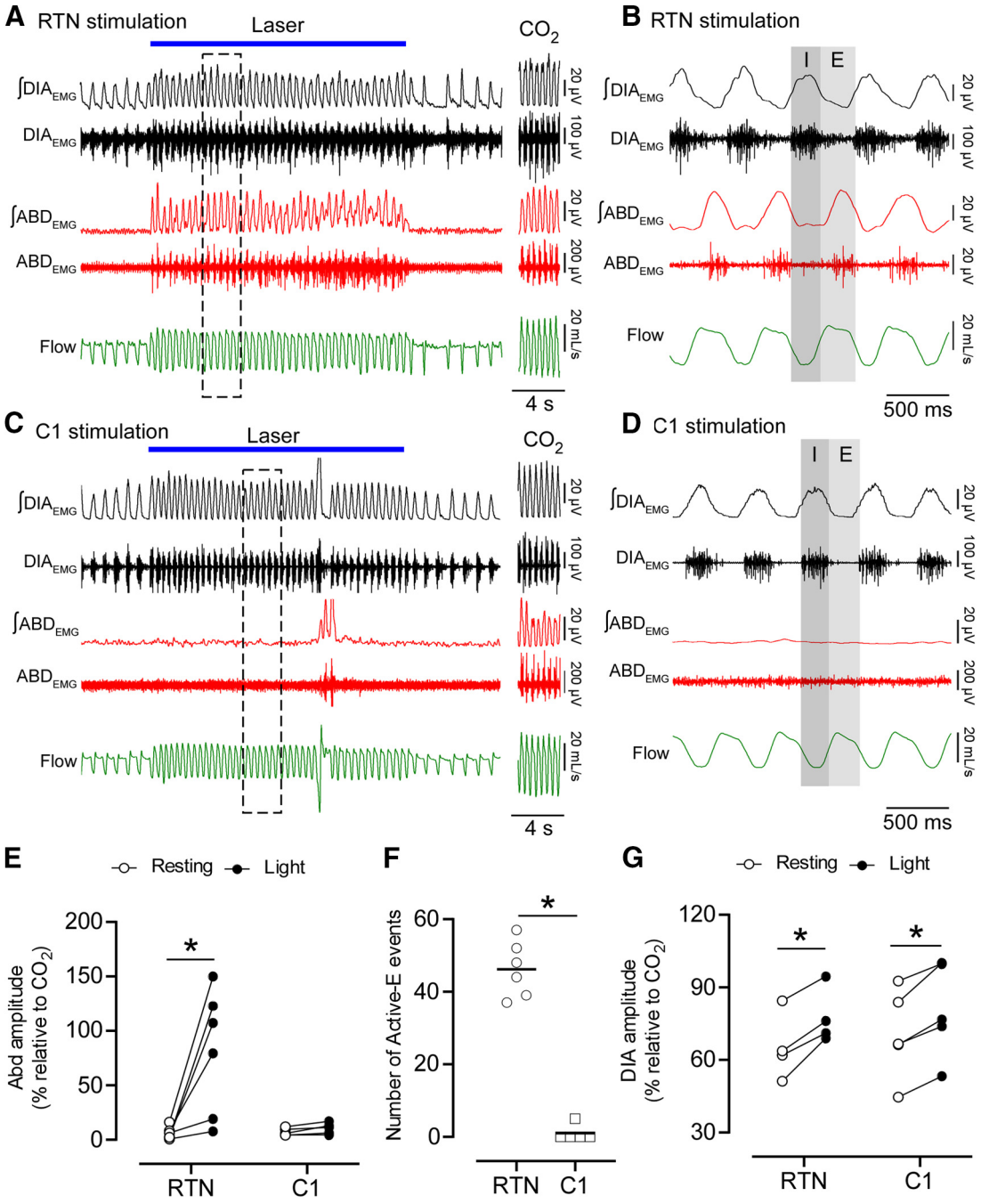

Figure 3. RTN stimulation drives active expiration in unanesthetized freely behaving rats. ***A-D***, DIA_{EMG}, ABD_{EMG} and flow recordings. ***A***, Selective RTN stimulation. During the laser stimulation, an increase in ventilation is associated with the immediate recruitment of rhythmic ABD_{EMG}. ABD_{EMG} was also increased and rhythmic during sustained hypercapnia (***A***, right; $F_ICO_2 = 0.09$). ***B***, Magnification of five respiratory cycles (***A***, dashed outline) during laser stimulation of RTN neurons. ABD_{EMG} activity is phase-locked in expiration (E). I, Inspiration. ***C***, Selective C1 stimulation. Note the increase in ventilation compared with ***A***, but without increased ABD_{EMG}. ABD_{EMG} was increased and rhythmic during hypercapnia ($F_ICO_2 = 0.09$). ***D***, Magnification of five respiratory cycles (***C***, dashed outline) during laser stimulation. Note the absence of rhythmic activity in ABD_{EMG} compared with ***B***. ***E***, Changes in ABD_{EMG} amplitude (relative to maximum obtained under CO_2) in response to RTN ($n = 6$) or C1 ($n = 5$) stimulation. ANOVA two-way for repeated measures: interaction between cell type and stimulation, $F_{(1,9)} = 8.443$, $p = 0.017$; cell type effect, $F_{(1,9)} = 6.380$, $p = 0.032$; stimulation effect, $F_{(1,9)} = 10.04$, $p = 0.011$. Bonferroni's multiple comparisons (resting vs stimulation): RTN, $p = 0.003$; C1, $p > 0.99$. ***F***, Absolute number of active expiration events observed during 20 s of stimulation. Mann–Whitney: RTN vs C1, $p = 0.004$. ***G***, DIA_{EMG} amplitude in response to RTN ($n = 4$) or C1 ($n = 5$) stimulation. ANOVA two-way for repeated measures: interaction between cell type and stimulation, $F_{(1,2)} = 0.926$, $p = 0.434$; cell type effect, $F_{(1,4)} = 0.147$, $p = 0.720$; stimulation effect, $F_{(1,4)} = 76.2$, $p = 0.0009$. Bonferroni multiple comparisons (resting vs stimulation): RTN, $p = 0.001$; C1, $p = 0.002$. *$p < 0.05$ (Bonferroni's multiple comparisons or Mann–Whitney; ***F***).

number of mCherry neurons identified in a 1 in 6 series of transverse sections, 60.6 ± 12.0% of RTN neurons expressed ChR2-mCherry on the left side of the brain (range: 40%–79.3%; $n = 10$). Transduced RTN neurons were observed across the entire area of distribution of *Nmb* neurons and included the regions defined by others as ventral and lateral parafacial groups (Fig. 1*C*,*E*). As expected (Souza et al., 2019), neurons expressing *Th* mRNA close to the injection site were eliminated following injections of Cre-dependent TevP-Casp3, and thus virtually none of the ChR2-expressing neurons was catecholaminergic (1 *Th* neuron found in 51 sections from 4 cases examined). *Th* neurons were observed in the contralateral rostral ventrolateral medulla, and other sites

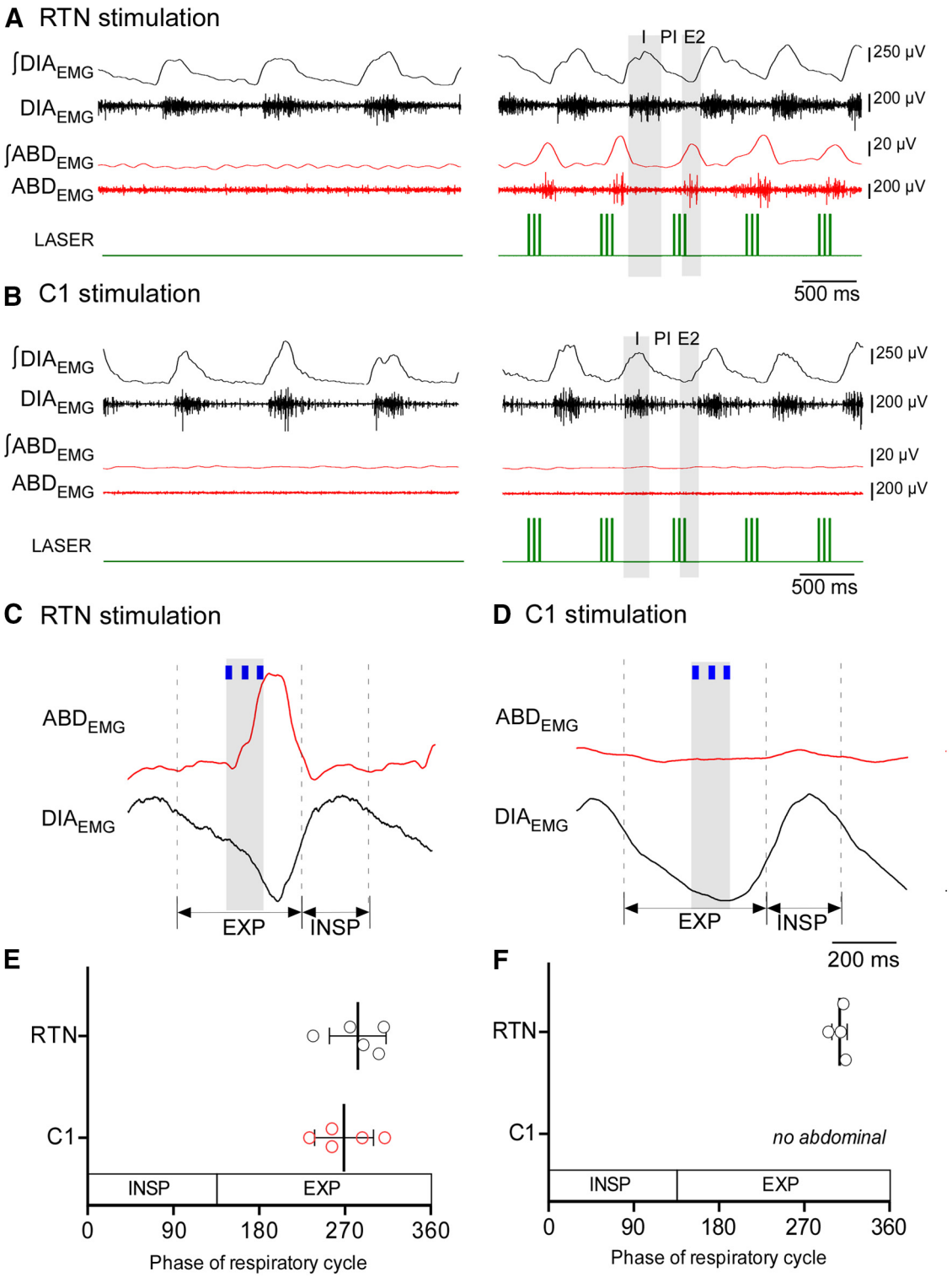

Figure 4. Stimulation of RTN neurons entrains the respiratory cycle and induces active expiration. ***A***, DIA_{EMG} and ABD_{EMG} during phasic stimulation of RTN neurons. Phasic stimulation (1.5 Hz) entrains the respiratory cycle and triggers a burst of ABD_{EMG} in the late-expiratory phase (E2). ***B***, DIA_{EMG} and ABD_{EMG} during phasic stimulation of C1 neurons. C1 phasic stimulation entrains the respiratory cycle but does not elicit active expiration. I, Inspiration; PI, post inspiration (also known as E1 phase); E2, late-expiratory phase. ***C***, Waveform averages of DIA_{EMG} and ABD_{EMG} showing the relationship between the phase of the respiratory cycle and the entrainment stimulus for RTN cases. ***D***, Waveform averages of DIA_{EMG} and ABD_{EMG} showing the relationship between the phase of respiratory cycle and the entrainment stimulus for C1 cases. ***E***, Respiratory cycle represented in 360° showing the phase of the respiratory cycle when stimulus entrains breathing for RTN ($n = 5$) and C1 ($n = 5$) stimulation. Student's *t* test: RTN versus C1, $p = 0.4735$. ***F***, Phase angle of the ABD_{EMG} peak elicited by phasic RTN stimulation. In 1 rat, phasic RTN stimulation entrained the respiratory cycle but did not activate ABD_{EMG}. In this animal, active expiration occurred only during 20 Hz continuous stimulation.

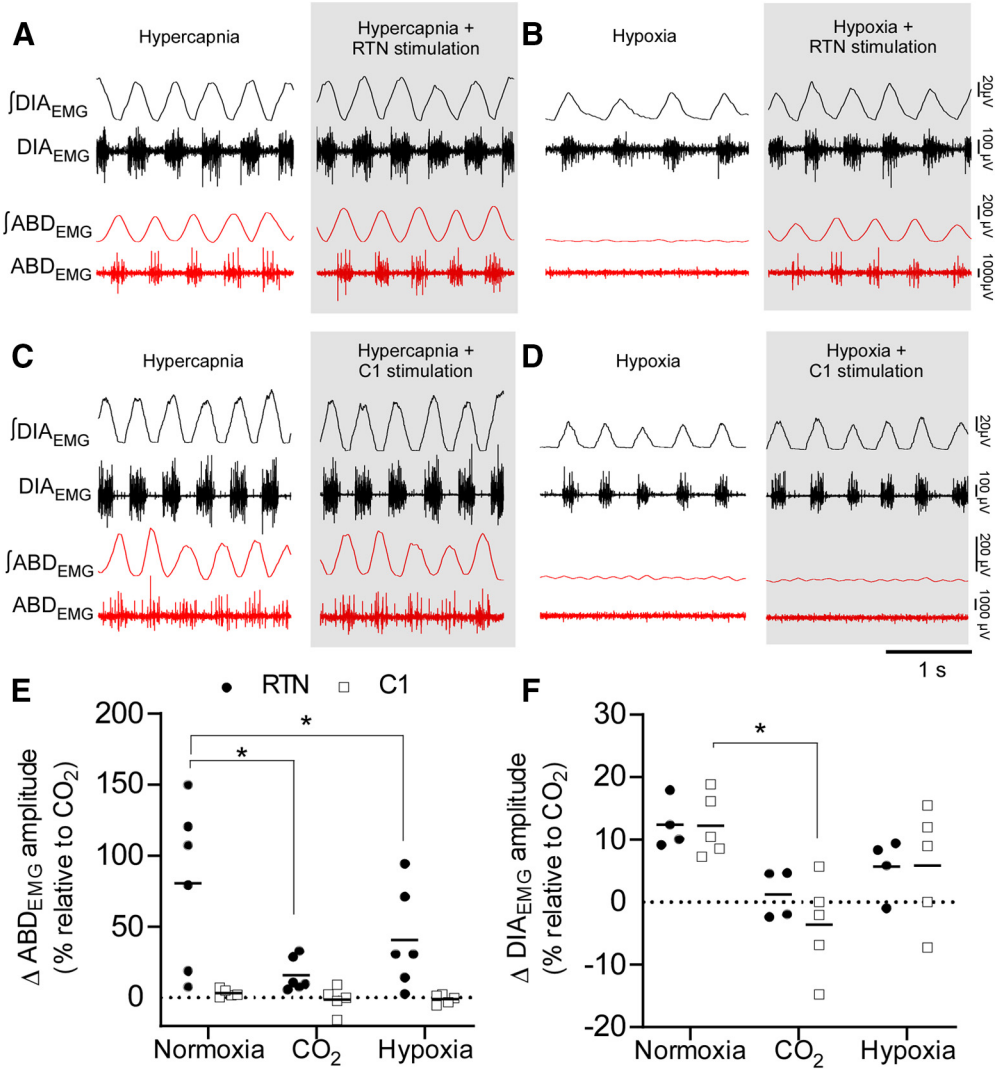

Figure 5. Hypercapnia, but not hypoxia, occludes the effects of RTN stimulations on DIA_{EMG} and ABD_{EMG}. ***A***, Sustained hyperoxic hypercapnia ($F_ICO_2 = 0.09$; $F_IO_2 = 0.65$) increases ABD_{EMG} and DIA_{EMG} amplitude. Hypercapnia occluded the recruitment of ABD_{EMG} and DIA_{EMG} during RTN stimulation (gray). ***B***, Sustained hypoxia ($F_IO_2 = 0.12$) does not elicit active expiration in freely behaving rats. RTN stimulation (gray) induces active expiration under hypoxia. ***C***, Sustained hypercapnia ($F_ICO_2 = 0.09$) increases ABD_{EMG} and DIA_{EMG} amplitude. C1 stimulation during hypercapnia (gray) had no further effect on ABD_{EMG} or DIA_{EMG}. ***D***, C1 neuron stimulation under hypoxia (gray) does not produce active expiration. ***E***, Changes in ABD_{EMG} amplitude during RTN or C1 neuron stimulation in three conditions: normoxia ($F_ICO_2 = 0.0$; $F_IO_2 = 0.21$), hyperoxia hypercapnia ($F_ICO_2 = 0.09$; $F_IO_2 = 0.65$), and hypoxia ($F_ICO_2 = 0.0$; $F_IO_2 = 0.12$). ANOVA two-way repeated measures: interaction between cell type and gas mixture, $F_{(2,18)} = 4.536$, $p = 0.0254$; effect of cell type, $F_{(2,18)} = 6.098$, $p = 0.0095$; effect of gas mixture, $F_{(1,9)} = 11.2$, $p = 0.0086$. Bonferroni's multiple comparisons for RTN: normoxia versus CO_2, $p = 0.0005$; normoxia versus hypoxia, $p = 0.0256$; CO_2 versus hypoxia, $p = 0.2533$. Bonferroni multiple comparisons for C1: normoxia versus CO_2, $p > 0.99$; normoxia versus hypoxia, $p > 0.99$; CO_2 versus hypoxia, $p > 0.99$. ***F***, Changes in DIA_{EMG} amplitude during RTN or C1 neuron stimulation in three conditions: room air, hypercapnia, and hypoxia. ANOVA two-way repeated measures: interaction between cell type and gas mixture, $F_{(2,5)} = 0.43$, $p = 0.671$; effect of cell type, $F_{(1,4)} = 0.42$, $p = 0.549$; effect of gas mixture, $F_{(2,8)} = 10.1$, $p = 0.006$. Bonferroni's multiple comparisons for C1: normoxia vs CO_2, $p = 0.0049$. $^*p < 0.05$ (Bonferroni's multiple comparisons).

known to contain *Th* neurons (not shown), suggesting the lesion of TH neurons was restricted to the injection site.

Five to 6 weeks after injection of AAV_2-DIO-ChR2(H134R)-eYFP into the rostral ventrolateral medulla, most eYFP-immunoreactive neurons contained *Th* mRNA (74.8 ± 5.5%, range: 67.7%-85.3%, $n = 6$; Fig. 1*B*), indicating their catecholaminergic nature, whereas eYFP-immunoreactive neurons containing *Nmb* mRNA were extremely rare (only 3 neurons in total found in 50 sections from 5 cases examined). *Th* neurons expressing ChR2 were distributed over a region spanning ~1.8 mm caudal to the caudal pole of the facial nucleus extending to 400 µm rostral to that point (Fig. 1*D*,*F*). Within the rostral ventrolateral medulla, 75.5 ± 7% of the *Th* neurons ($n = 3$, range: 67.6%–85.5%) contained detectable eYFP-immunoreactivity.

Selective stimulation of RTN or C1 neurons increases ventilation

Tonic stimulation of RTN or C1 neurons (20 Hz, 10 ms pulse, 20 s) increased f_R, V_T, and V_E to a comparable degree (Fig. 2*A*–*C*). In cases targeting the RTN, the increase in V_E (ΔV_E) was positively correlated with the number of *Nmb* neurons expressing ChR2 (Fig. 2*D*), whereas no correlation between ΔV_E and the number *Th* neurons expressing ChR2 was observed in cases targeting C1 neurons (Fig. 2*E*).

Selective stimulation of RTN neurons, but not C1 neurons, induces active expiration in unanesthetized rats

Tonic optogenetic stimulation of RTN neurons (20 Hz, 20 s, 10 ms pulses) reliably elicited active expiration (burst of

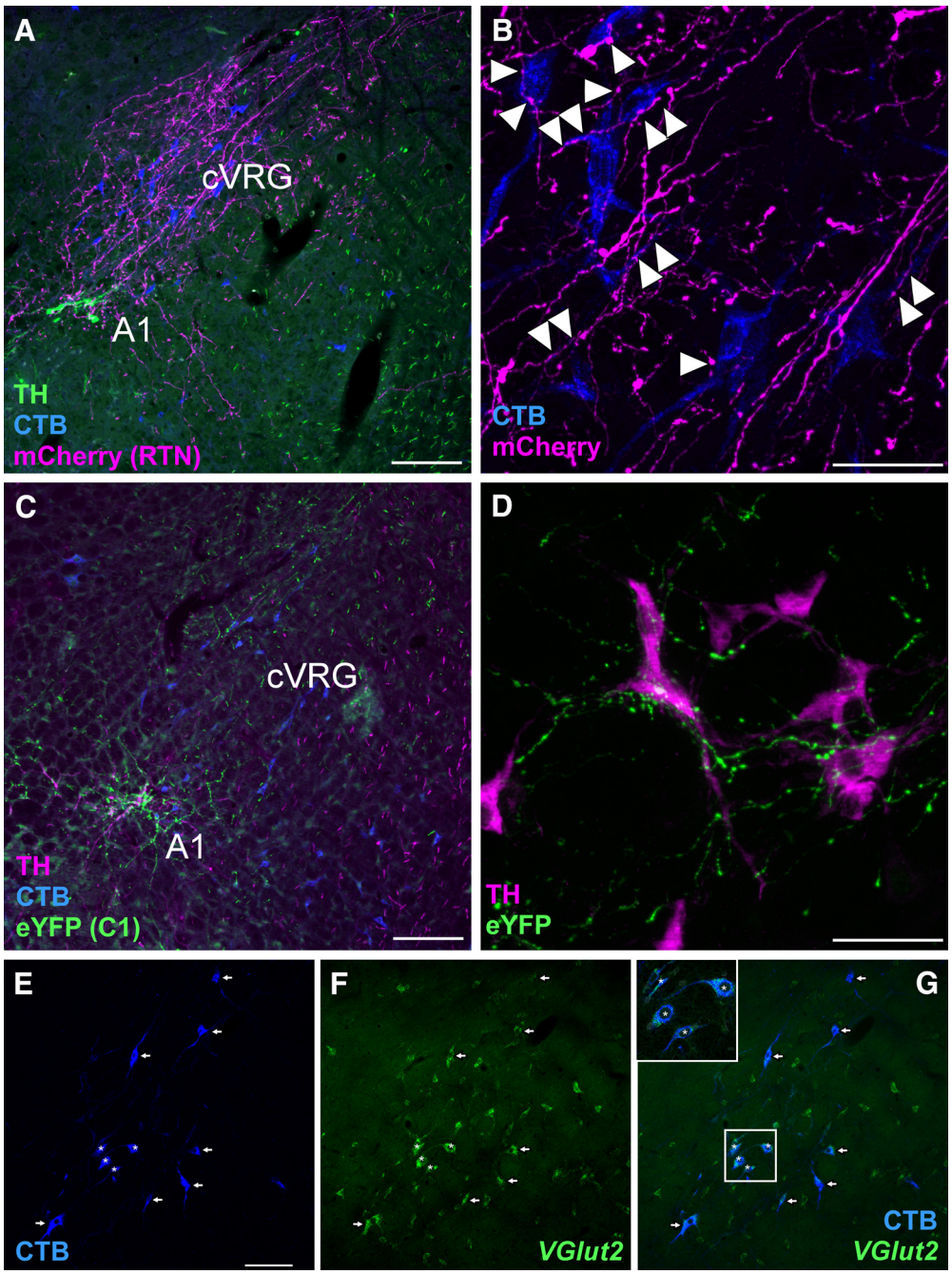

Figure 6. RTN and C1 projections to the cVRG and A1 region. ***A***, Transverse section (left; −14.40 mm relative to bregma) showing a dense projection from RTN neurons (fibers in magenta; mCherry) to putative abdominal premotor neurons retrogradely with CTB (blue) in the cVRG. ***B***, High-magnification photomicrography showing close appositions (arrowheads) between RTN fibers (magenta; mCherry) and CTB-labeled neurons (blue). ***C***, Photomicrography showing the sparse projection of C1 neurons (green fibers; eYFP) to the cVRG. Instead, C1 neurons densely project to the noradrenergic neurons of the A1 group. ***D***, High magnification showing C1 neurons with close appositions (green fibers; $eYFP^+$) onto A1 neurons (magenta; TH^+). ***E***, Bulbospinal neurons labeled with CTB in the cVRG. ***F***, *Slc17a6* (*VGlut2*) mRNA by ISH. ***G***, Merge of ***E*** and ***F***, indicating that virtually all cVRG neurons with projection to lower thoracic and upper lumbar level of spinal cord express *VGlut2*. Top left, Inset, Neurons marked with asterisks showing higher detail. Arrows and asterisks indicate double-labeled neurons. Scale bars: ***A***, ***C***, 100 μm; ***B***, ***D***, 50 μm; ***E***, 100 μm.

ABD_{EMG} during the E2 phase) in unanesthetized freely behaving rats breathing room air ($n = 6$; Fig. 3*A*,*B*). In 4 rats, the amplitude of the ABD_{EMG} during RTN stimulation in normocapnic conditions was similar or greater than that elicited by hyperoxic hypercapnia (F_ICO_2 = 0.09; Fig. 3*E*). In the other 2 cases, ABD_{EMG} amplitude during photostimulation in normocapnic conditions was less than during hypercapnia; however, the frequency of active expiration events (i.e., the number of respiratory cycles in which active expiration was evident) was similar during RTN stimulation in all cases regardless of the change in ABD_{EMG} amplitude (Fig. 3*F*). RTN stimulation also increased DIA_{EMG} amplitude (Fig. 3*G*). Tonic C1 neuron stimulation increased f_R and DIA_{EMG} amplitude to a degree comparable to RTN stimulation, but active expiration was not observed (Fig. 3*C*,*D*).

Phasic stimulation of either RTN or C1 neurons at 1.5 Hz entrained the breathing cycle (Fig. 4*A*–*D*). In both cases, the stimuli occurred at the transition between the postinspiratory (E1) and late-expiratory (E2) phases (Fig. 4*C*–*E*). Active

expiration was only observed during RTN stimulation (Fig. 4*A–F*). This burst occurred immediately after the stimulus (Fig. 4*C*,*F*).

Hyperoxic hypercapnia (F_ICO_2 = 0.09; F_IO_2 = 0.65) induced active expiration in all rats (Fig. 5*A*,*C*). Under hypercapnic conditions when active expiration was evident, RTN stimulation produced a negligible further increase in ABD_{EMG} and DIA_{EMG} amplitudes (Fig. 5*A*,*E*,*F*). During hypoxia (F_IO_2 = 0.12), ABD_{EMG} oscillations were not observed, but RTN stimulation still induced active expiration (Fig. 5*B*,*E*). C1 neuron stimulation failed to produce or enhance active expiration under hypercapnia or hypoxia (Fig. 5*C*,*D*).

Finally, we found that RTN neurons densely innervated the ipsilateral cVRG (Fig. 6*A*), defined by the presence of glutamatergic neurons with projections to the lower thoracic and lumbar spinal cord (Iscoe, 1998). We observed close appositions between RTN boutons and bulbospinal cVRG neuronal processes (Fig. 6*B*). The vast majority of the bulbospinal neurons located in the cVRG (94.4 ± 0.8%, counted in 5 sections from 3 cases) contained *VGlut2* mRNA (Fig. 6*E–G*) and therefore were presumptive excitatory abdominal premotor neurons (Iscoe, 1998). By contrast, the cVRG receives a very light projection from C1 neurons (Fig. 6*C*), which preferentially target the A1 catecholaminergic group at this level of the ventrolateral medulla (Fig. 6*D*). No RTN projections to the thoracic and lumbar spinal cord were observed. In summary, RTN stimulation elicits active expiration and innervates abdominal excitatory premotor neurons located within the cVRG, whereas C1 neurons do neither.

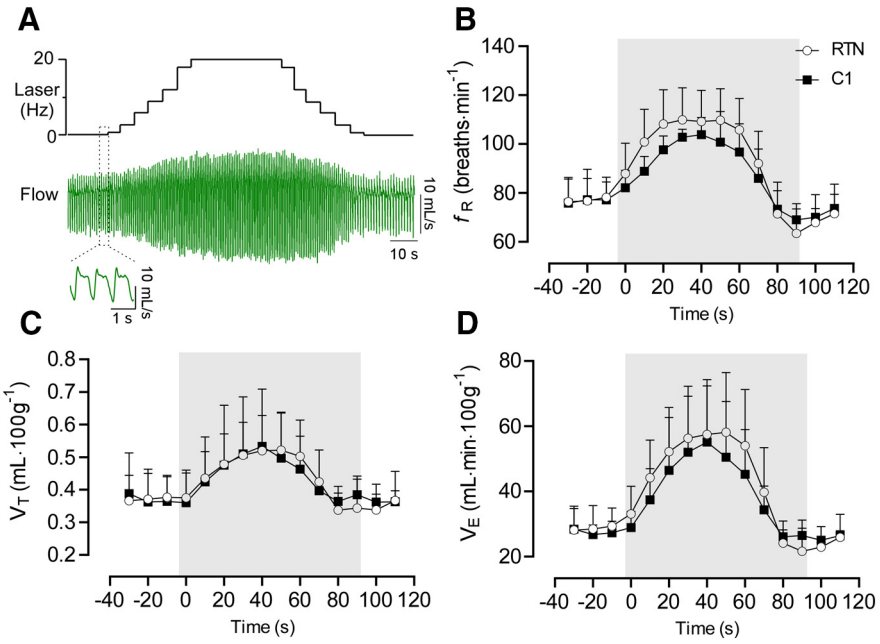

Figure 7. Respiratory changes during incrementing-decrementing stimulation of RTN (n = 8) or C1 (n = 6). ***A***, Respiratory flow during RTN or C1 stimulation. This pattern of stimulation produces a smooth increase in the respiratory variables mimicking the pattern of breathing during acute CO_2 or hypoxia exposure (Souza et al., 2019). ***B***, Average values from f_R incrementing-decrementing stimulation. Two-way ANOVA for repeated measures: interaction between cell type and time, $F_{(14,168)}$ = 1.07, p = 0.3866; effect of time, $F_{(2.85,34.3)}$ = 56.6, $p < 0.0001$; effect of cell type, $F_{(1,12)}$ = 1.54, p = 0.2337. ***C***, V_T. Two-way ANOVA for repeated measures: interaction between cell type and time, $F_{(14,168)}$ = 0.70, p = 0.7671; effect of time, $F_{(2.3,27.9)}$ = 23.3, $p < 0.0001$; effect of cell type, $F_{(1,12)}$ = 0.43, p = 0.5236. ***D***, V_E. Two-way ANOVA for repeated measures: interaction between cell type and time, $F_{(14,168)}$ = 0.68, p = 0.7825; effect of time, $F_{(1.3,15.6)}$ = 52.7, $p < 0.0001$; effect of cell type, $F_{(1,12)}$ = 0.008, p = 0.9266.

Selective stimulation of RTN and C1 neurons induces arousal from sleep

We used an incrementing-decrementing pattern of photostimulation to emulate the gradual increase in RTN neuronal activity that would result from an acute reduction in alveolar ventilation and the resulting slow accumulation of CO_2 (Fig. 7*A*). This stimulation was applied while the rats were in NREM sleep; it increased f_R, V_T, and V_E to the same degree regardless of whether RTN or C1 was stimulated (Fig. 7*B–D*). RTN stimulation significantly increased the probability of arousal from NREM sleep (no stimulation vs RTN stimulation: 71.6 ± 12.6% vs 48.2 ± 13.1% probability to remain asleep following 50 s of stimulation; Fig. 8*A*,*B*). However, arousal induced by RTN stimulation was modest compared with that induced by C1 stimulation (no stimulation vs C1 stimulation: 63.0 ± 17% vs 6.7 ± 12.1% probability to remain asleep in 50 s of stimulation; Fig. 8*A*,*C*). Overall, the sleep probability curves were significantly different between RTN and C1 neurons (two-way ANOVA: interaction between cell type and time, $F_{(13,156)}$ = 10.9, $p < 0.0001$; effect of cell type, $F_{(1,12)}$ = 27.8, p = 0.0002; effect of time, $F_{(3.4,41.6)}$ = 144.5, $p < 0.0001$). Moreover, arousal lasted longer following C1 neuron stimulation than following RTN stimulation (92.5 ± 16.7 vs 35.4 ± 5.8 s) (two-way ANOVA for repeated measures: interaction between cell type and stimulation, $F_{(1,24)}$ = 17.2, p = 0.0004; effect of cell type, $F_{(1,24)}$ = 21.1, p = 0.0001; effect of stimulation, $F_{(1,24)}$ =37.5, $p < 0.0001$; Bonferroni's post-test, $p < 0.0001$). By contrast, the duration of waking following a spontaneous arousal was similar in both groups (RTN vs C1, 33.1 ± 13.0 vs 44.0 ± 21.1 s, Bonferroni's post-test, p = 0.3511) Consistent with previous work (Burke et al., 2015a), C1 stimulation increased the probability of sighing, whereas RTN stimulation did not (Fig. 8*D*,*E*) (two-way ANOVA for repeated measures: interaction between cell type and stimulation, $F_{(1,24)}$ = 17.2, p = 0.0004; effect of cell type, $F_{(1,24)}$ = 37.5, $p < 0.0001$; effect of stimulation, $F_{(1,24)}$ = 21.0, p = 0.0001). Laser light itself had no effect on arousal probability or sighing (Fig. 9); therefore, the arousal elicited by delivering light to the ventrolateral medulla required expression of ChR2 by RTN or C1 neurons.

The above physiological evidence suggests that both RTN and C1 neurons promote arousal, but C1 neurons provide a substantially stronger input to arousal systems. Consistent with this view, RTN projections were very rarely observed rostral to parabrachial complex (PB), with no fibers observed rostral to the caudal periaqueductal gray. In the PB region, the densest RTN innervation was to the ipsilateral Kölliker-Fuse and lateral crescent nuclei (Fig. 10*A1–A3*). RTN fibers were not observed in the core of the external lateral nucleus of the PB (PBel) defined here by the presence of CGRP immunoreactivity (Palmiter, 2018); however, terminal fields of RTN neurons surrounded the PBel (Fig. 10). There was no innervation of the dorsal raphe and pedunculopontine nucleus (data not shown), and RTN fibers were negligible within the LC and peri-LC region (Fig. 10*A1–A3*). In stark contrast, the axonal varicosities of C1 neurons clearly formed close appositions with CGRP-immunoreactive

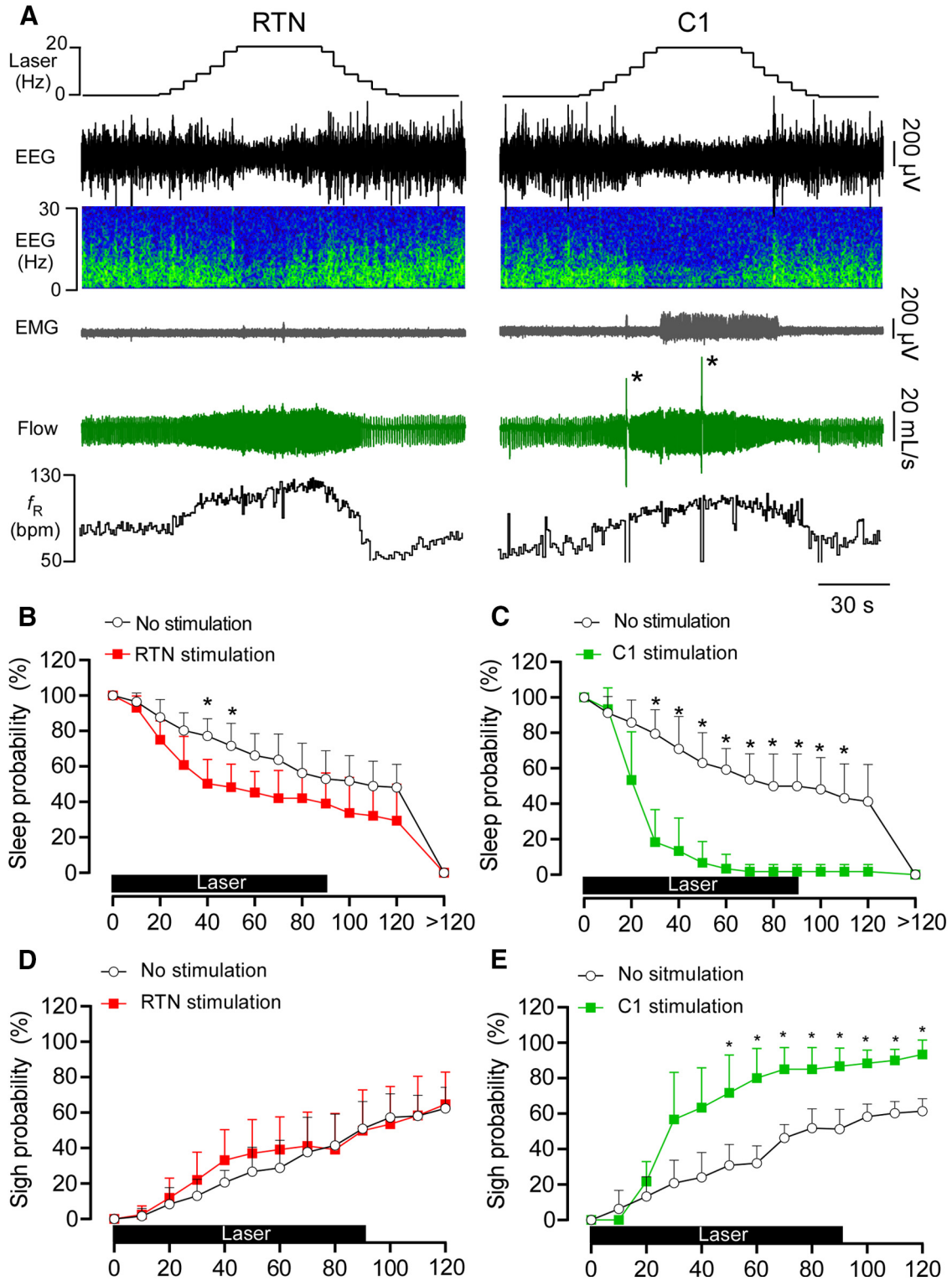

Figure 8. RTN or C1 stimulation causes arousal from sleep. ***A***, EEG, neck EMG, and breathing during augmenting RTN and C1 stimulation. Note the period of arousal in both examples denoted by EEG desynchronization. Also, the period of wakefulness is longer following C1 stimulation than RTN stimulation, and C1 but not RTN stimulation results in sighs (asterisks). ***B***, Sleep probability curves during RTN stimulation ($n = 8$) or dummy stimulation (representing the probability of a spontaneous arousal). ANOVA two-way repeated measures: interaction between stimulation and time, $F_{(13,182)} = 3.857$, $p < 0.0001$; effect of time, $F_{(2.7,37.7)} = 138.4$, $p < 0.0001$; effect of stimulation, $F_{(1,14)} = 8.796$, $p = 0.0102$. ***C***, Sleep probability curves during C1 stimulation ($n = 6$) and dummy stimulation. ANOVA two-way repeated measures: interaction between stimulation and time, $F_{(13,130)} = 17.5$, $p < 0.0001$; effect of time, $F_{(3.9,39.4)} = 110.6$, $p < 0.0001$; effect of stimulation, $F_{(1,10)} = 44.02$, $p < 0.0001$. ***D***, Sigh probability curves during RTN stimulation ($n = 8$) and dummy stimulation. ANOVA two-way repeated measures: interaction between stimulation and time, $F_{(12,168)} = 1.34$, $p = 0.2014$; effect of time, $F_{(2.8,39.9)} = 82.2$, $p < 0.0001$; effect of stimulation, $F_{(1,14)} = 0.32$, $p = 0.5796$. ***E***, Sigh probability curves during C1 stimulation ($n = 6$) and dummy stimulation. ANOVA two-way repeated measures: interaction between stimulation and time, $F_{(12,120)} = 8.43$, $p < 0.0001$; effect of time, $F_{(3.1,31.7)} = 89.8$, $p < 0.0001$; effect of stimulation, $F_{(1,10)} = 39.4$, $p < 0.0001$. *$p < 0.05$ (Bonferroni's multiple comparisons between stimulation and no stimulation in ***B-E***).

processes in the caudal PB (Fig. 10*B1*), and sparsely innervated the PBel nucleus. Bilateral innervation of the dorsal and medial PB was also notable, whereas the Kölliker-Fuse was essentially devoid of C1 neuron fibers and terminals. C1 innervation of the LC and peri-LC was dense (Fig. 10*B1–B3*), consistent with prior electrophysiological and ultrastructural evidence of a monosynaptic input from C1 to the LC neurons in mice (Abbott et al., 2012; Holloway et al., 2013). We also observed sparse innervation from C1 neurons to the dorsal raphe and pedunculopontine nucleus and a heavy innervation of the ventrolateral periaqueductal gray (not shown).

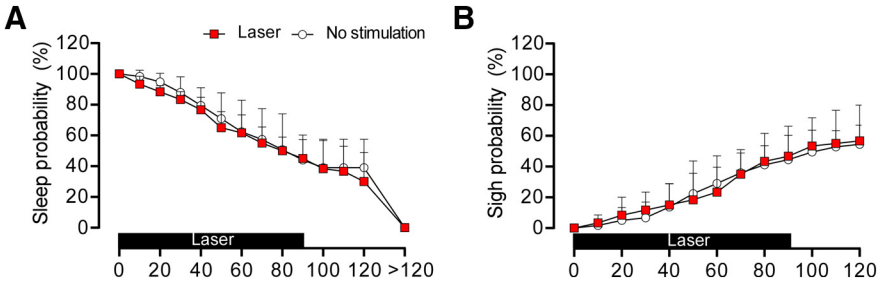

Figure 9. ***A***, Laser light itself does not affect arousal probability ($n = 6$). ANOVA two-way repeated measures: interaction between laser and time, $F_{(13,130)} = 0.267$, $p = 0.9949$; effect of time, $F_{(13,130)} = 98.8$, $p < 0.0001$; effect of laser light, $F_{(1,10)} = 0.289$, $p = 0.6024$. ***B***, Laser light itself does not affect sighing probability ($n = 6$). ANOVA two-way repeated measures: interaction between laser and time, $F_{(13,130)} = 0.328$, $p = 0.9865$; effect of time, $F_{(13,130)} = 114.4$, $p < 0.0001$; effect of laser light, $F_{(1,10)} = 0.02$, $p = 0.8901$.

Discussion

We demonstrate the following: selective activation of RTN or C1 neurons increases breathing frequency and amplitude; only RTN produces active expiration and only C1 triggers sighs; RTN, but not C1 neurons, innervates abdominal premotor neurons; and C1 neurons produce stronger arousal than RTN and heavily innervate arousal-promoting pontomedullary regions.

Selective RTN photostimulation produces active expiration

Based on plethysmography evidence, RTN neuron stimulation raises f_R, enhances inspiration, and probably recruits active expiration (Abbott et al., 2011). Similar conclusions have been reached by others (Marina et al., 2010; Cregg et al., 2017). These studies could not exclude a contribution of the C1 neurons to these effects. Here, in freely behaving rats, we show that selective activation of RTN neurons elicits a breathing response that is indistinguishable from the effect of hypercapnia, including robust active expiration and arousal. Under normoxia, C1 stimulation increased breathing but did not produce active expiration (present data), although under severe hypoxia C1 may facilitate active expiration (Malheiros-Lima et al., 2020). The anatomic evidence revealed a key difference: RTN innervates bulbospinal expiratory premotor neurons, C1 does not.

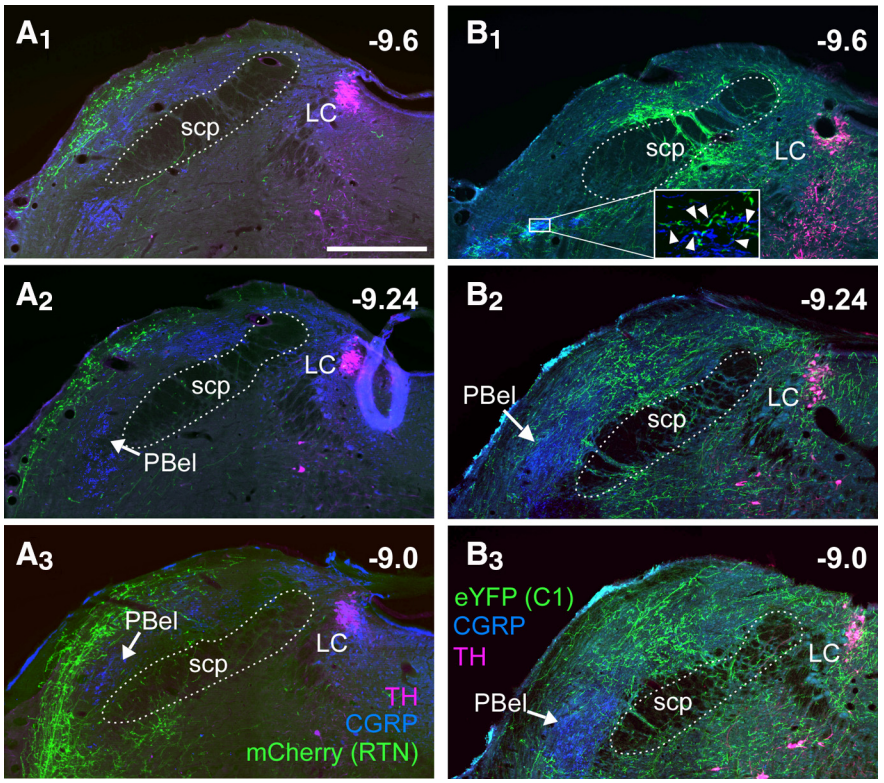

Figure 10. Projections of RTN and C1 neurons to the PB and LC. ***A1-A3***, Coronal sections at three rostrocaudal levels showing the projections of RTN neurons expressing mCherry (fibers in green). The PBel is identified by the presence of CGRP immunoreactivity (blue). Magenta represents TH. ***B1-B3***, Coronal sections at three rostrocaudal levels showing the projection of C1 neurons (eYFP$^+$ fibers, in green) to the PB. Blue represents CGRP. Magenta represents TH. Note the overlap between C1 fibers and CGRP processes in the caudal portion of PBel (***B1***, boxed area and magnified inset; arrowheads) and the dense innervation to LC.

Mechanism of RTN-triggered active expiration

The discharge of expiratory premotor neurons is largely defined by phasic inspiratory and postinspiratory inhibition from pontomedullary respiratory centers and by a heretofore elusive CO_2-dependent excitatory drive (Bainton and Kirkwood, 1979; Iscoe, 1998). The latter input likely originates from RTN for the following reasons (Fig. 11). RTN neurons are powerfully activated by hypercapnia (Guyenet et al., 2019); hypercapnia and selective optical activation of RTN have the same effect on abdominal muscle contractions, and the effect of RTN stimulation is occluded by hypercapnia. Finally, RTN neurons, which are 100% glutamatergic, densely innervate the region of the lower medulla that contains the excitatory abdominal premotor neurons (Abbott et al., 2011; present study).

Tonic 20 Hz activation of ChR2-expressing RTN neurons reproduces faithfully the effect of hypercapnia in unanesthetized rats; therefore, phasic activation of RTN neurons is not required for these cells to activate the various motor outflows, including abdominal muscles, during the appropriate phase of the respiratory cycle. Under anesthesia, neurochemically identified (Phox2b$^+$) RTN

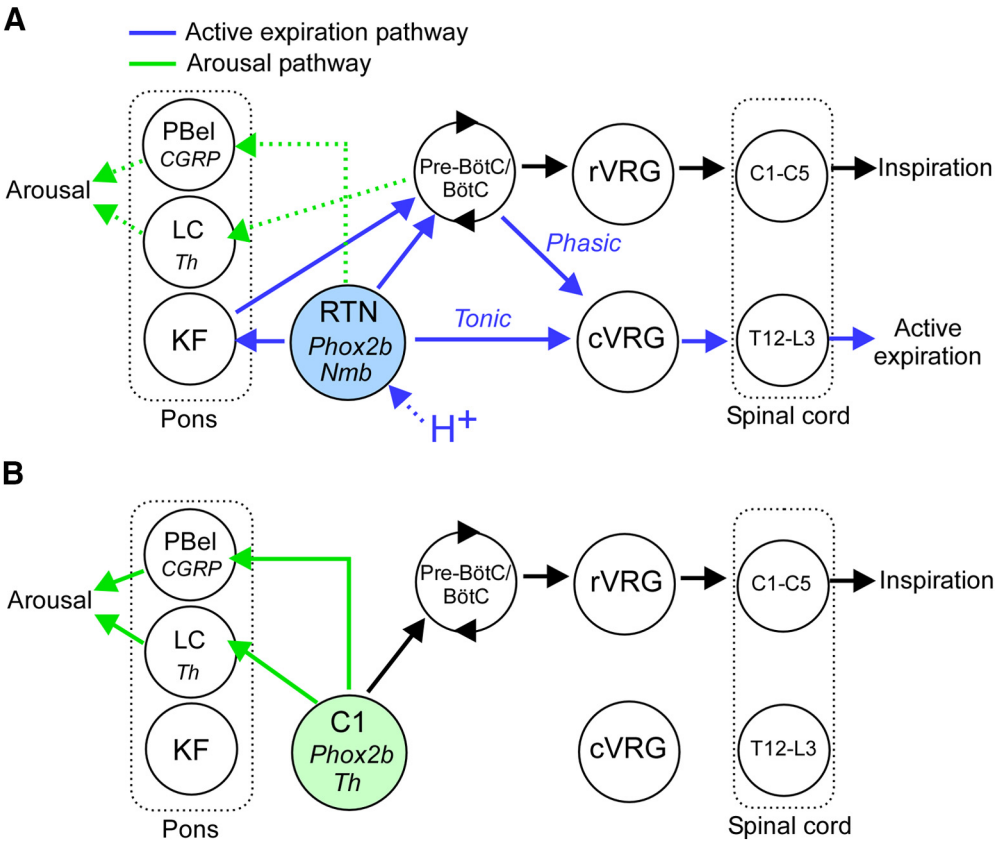

Figure 11. Hypothesis for the generation of active expiration and arousal by RTN and C1 neurons. ***A***, RTN neurons (*Phox2b*+*Nmb*) promote active expiration via two mechanisms: a direct excitatory input to glutamatergic premotor neurons (cVRG) that drive abdominal muscle contractions via direct excitatory projections to spinal motor neurons and a shortening of the inhibition of the cVRG premotor neurons during the Post-I phase of the respiratory cycle. The latter mechanism probably relies on RTN projections to multiple segments of the respiratory pattern generator: Bötzinger (BötC), Pre-Bötzinger (Pre-BötC), and Kölliker-Fuse nucleus (Barnett et al., 2018). Inspiration is driven by RTN neurons via activation of the Pre-BötC (rate control), and inspiratory premotor neurons located in the rostral ventral respiratory group (rVRG; amplitude control). The modest arousal potential of the RTN may rely on direct inputs to the PBel or by pathways associated with breathing activation, that is, via excitation of central respiratory centers or changes in sensory feedback stimulated by increased lung ventilation. ***B***, C1 neurons may promote arousal through dense projections to the *Th* neurons of the LC, CGRP neurons in the PBel, and hypothalamic regions (data not shown). C1 neurons do not project to cVRG expiratory premotor neurons and therefore do not effectively stimulate active expiration. However, C1 neurons are capable of stimulating breathing and sighs possibly through their connections with BötC/Pre-BötC.

neurons discharge throughout the respiratory cycle and have varying degrees of respiratory modulation at higher F_ICO_2, but a late-expiratory augmenting pattern has not been reported. Their respiratory modulation is attributed to feedback from lung afferents and the respiratory pattern generator (Guyenet et al., 2005; Moreira et al., 2007).

The RTN projection to the Bötzinger region could also contribute to active expiration by shortening the discharge of the Post-I neurons that inhibit the premotor neurons during early expiration (Smith et al., 2013; Flor et al., 2020). This shortening could result from the excitation by RTN of the augmenting-expiratory inhibitory neurons located in the same brain region.

RTN and the parafacial expiratory oscillator

The region located beneath the facial motor nucleus has been subdivided in two parts by some authors (Huckstepp et al., 2015; Del Negro et al., 2018; Pisanski and Pagliardini, 2019). The lateral portion dubbed pF_L (Huckstepp et al., 2015; Del Negro et al., 2018) or parafacial respiratory group (pFRG) (Pisanski and Pagliardini, 2019), is believed to contain an oscillator required for active expiration and the medial portion (ventral parafacial nucleus [pF_V]), are chemoreceptors (Huckstepp et al., 2015; Del Negro et al., 2018). According to this theory, the pF_L/pFRG oscillator consists of neurons other than RTN, whereas pFv includes RTN (Huckstepp et al., 2015). The pF_L/pF_V subdivision is an interpretation of the differential effects produced in an anesthetized preparation by local microinjections of nonselective disinhibitory drugs (bicuculline/strychnine) or the use of neuronal actuators delivered locally using pan-neuronal vectors (Pagliardini et al., 2011; Huckstepp et al., 2015; Pisanski et al., 2020). The phenotype and connectome of the neurons that constitute the pF_L/pFRG are unidentified. Candidates include neurons that discharge very briefly before the phrenic nerve (Pagliardini et al., 2011; de Britto and Moraes, 2017). These neurons do not express Phox2b and thus are indeed different from RTN (de Britto and Moraes, 2017), but there is currently little evidence that these particular neurons drive active expiration since they cannot yet be selectively manipulated and their axonal projections are unknown. The region defined as pF_L/pFRG actually contains many RTN cell bodies and the dendrites of more medially located RTN neurons (Abbott et al., 2011; Shi et al., 2017; Guyenet et al., 2019; present study). Thus, the effects attributed to pF_L/pFRG neurons (Huckstepp et al., 2015; Pisanski et al., 2020) could have resulted from the activation of a subset of RTN neurons.

RTN, C1 neurons, and arousal

RTN stimulation causes arousal (present study) and RTN lesions attenuate CO_2-induced arousal (Souza et al., 2019); thus, CO_2-induced arousal relies partly on RTN activation. The arousal elicited by optogenetic RTN stimulation was relatively modest compared with the effect of CO_2 (Souza et al., 2019). However,

exposing animals to 10%-15% F_ICO_2, the usual protocol to examine CO_2-induced arousal, likely activates many more RTN neurons that the unilateral optical activation of this nucleus performed presently. In addition, the carotid bodies, cardiopulmonary and airway afferents, and acid-sensitive CNS structures other than RTN also contribute to hypercapnia-induced arousal (Gleeson et al., 1990; Berry and Gleeson, 1997; Buchanan and Richerson, 2010; Smith et al., 2018; Kaur and Saper, 2019; Souza et al., 2019). The relative contribution of these various factors to hypercapnia-induced arousal is presently uncertain.

As shown previously (Burke et al., 2014), C1 stimulation greatly increased arousal probability and produced long-lasting arousals. C1 stimulation caused much stronger arousal than RTN despite evoking a similar increase in breathing. Substantial projections from C1 to arousal-promoting regions of the pons, such as the PBel-CGRP neurons and locus ceruleus (LC), may account for the greater arousal potential of C1 versus RTN stimulation (Carter et al., 2010; Holloway et al., 2013; Bochorishvili et al., 2014; Kaur et al., 2017).

PBel-CGRP neurons mediate CO_2-induced arousal; therefore, we anticipated finding a direct projection from RTN to these pontine neurons (Kaur et al., 2017; Kaur and Saper, 2019). We did not clearly identify such contacts, perhaps because they occur on dendrites that were not detectable with our CGRP antibody. The dendrites of PBel neurons extend into the lateral crescent of the parabrachial nucleus (Chamberlin et al., 1999), which is heavily innervated by RTN (present study), and these distal dendrites also receive synaptic input from spinomedullary neurons (Cechetto et al., 1985; Bernard et al., 1994). Alternately, RTN neurons may promote arousal through neurons located elsewhere in the respiratory network.

C1, RTN, and sighs

Selective ChR2-mediated RTN stimulation did not produce sighs, and hypoxia-induced sighing is unaffected by virtually eliminating the RTN (Souza et al., 2018); therefore, our results do not support the view that *Nmb*-expressing RTN neurons contribute to the generation of sighs in rats (Li et al., 2016). A species difference could underlie the discrepancy, but the nature of the stimulus that induces sighing may be the key. Hypoxia may not stimulate NMB release by RTN neurons because this particular stimulus does not activate these neurons (Basting et al., 2015; Wakai et al., 2015). However, a subset of NMB-releasing RTN neurons may contribute to sighing induced by other stimuli (Li et al., 2020).

By contrast, we confirm that sighs are reliably produced by activating the C1 neurons (Burke et al., 2014). Catecholamines trigger sighs by activating a circuit located close to the core of the respiratory rhythm generator, the pre-Bötzinger complex (Viemari et al., 2013). C1 neurons may be a source of catecholamines to this region. However, sighs commonly occur during spontaneous arousals (Burke et al., 2014) and, as shown here, C1 stimulation causes arousal. The sighs elicited by C1 neuron stimulation could therefore be a remote consequence of arousal on the oscillator than generates the sighs.

Experimental limitations

The approach used here targeted the RTN with a high degree of selectivity; however, even minor off-target expression of ChR2 may have contributed to the effects we describe. Similarly, in the experiments designed to activate the C1 neurons, 25% of the ChR2-expressing neurons did not express *Th*, although these cells did not express *Nmb* and thus were not RTN neurons. Finally, C1 neurons were unilaterally eliminated in cases targeting the RTN, and these could conceivably contribute to arousal and sighs driven by RTN neurons (Burke et al., 2014; Malheiros-Lima et al., 2017).

In conclusion, RTN and C1 neurons regulate breathing and trigger arousal from sleep but with clear qualitative and quantitative differences (Fig. 11). RTN drives all aspects of breathing, including active expiration, consistent with its role in central respiratory chemoreflex. Neither optogenetic activation of RTN nor hypercapnia evokes sighs. Sighing may be elicited by a dedicated, possibly acid-insensitive, subset of RTN neurons. The powerful arousal elicited by C1 neuron stimulation is consistent with their postulated role in acute stress responses (Jansen et al., 1995; Guyenet et al., 2013).

References

Abbott SB, Stornetta RL, Fortuna MG, Depuy SD, West GH, Harris TE, Guyenet PG (2009) Photostimulation of retrotrapezoid nucleus phox2b-expressing neurons in vivo produces long-lasting activation of breathing in rats. J Neurosci 29:5806–5819.

Abbott SB, Stornetta RL, Coates MB, Guyenet PG (2011) Phox2b-expressing neurons of the parafacial region regulate breathing rate, inspiration, and expiration in conscious rats. J Neurosci 31:16410–16422.

Abbott SB, Kanbar R, Bochorishvili G, Coates MB, Stornetta RL, Guyenet PG (2012) C1 neurons excite locus coeruleus and A5 noradrenergic neurons along with sympathetic outflow in rats. J Physiol 590:2897–2915.

Abbott SB, Coates MB, Stornetta RL, Guyenet PG (2013) Optogenetic stimulation of C1 and retrotrapezoid nucleus neurons causes sleep state-dependent cardiorespiratory stimulation and arousal in rats. Hypertension 61:835–841.

Anderson TM, Ramirez JM (2017) Respiratory rhythm generation: triple oscillator hypothesis. F1000Res 6:139.

Bainton CR, Kirkwood PA (1979) The effect of carbon dioxide on the tonic and the rhythmic discharges of expiratory bulbospinal neurones. J Physiol 296:291–314.

Barnett WH, Jenkin SE, Milsom WK, Paton JF, Abdala AP, Molkov YI, Zoccal DB (2018) The Kölliker-Fuse nucleus orchestrates the timing of expiratory abdominal nerve bursting. J Neurophysiol 119:401–412.

Basting TM, Burke PG, Kanbar R, Viar KE, Stornetta DS, Stornetta RL, Guyenet PG (2015) Hypoxia silences retrotrapezoid nucleus respiratory chemoreceptors via alkalosis. J Neurosci 35:527–543.

Bernard JF, Huang GF, Besson JM (1994) The parabrachial area: electrophysiological evidence for an involvement in visceral nociceptive processes. J Neurophysiol 71:1646–1660.

Berry RB, Gleeson K (1997) Respiratory arousal from sleep: mechanisms and significance. Sleep 20:654–675.

Bochorishvili G, Nguyen T, Coates MB, Viar KE, Stornetta RL, Guyenet PG (2014) The orexinergic neurons receive synaptic input from C1 cells in rats. J Comp Neurol 522:3834–3846.

Buchanan GF, Richerson GB (2010) Central serotonin neurons are required for arousal to CO_2. Proc Natl Acad Sci USA 107:16354–16359.

Burke PG, Abbott SB, Coates MB, Viar KE, Stornetta RL, Guyenet PG (2014) Optogenetic stimulation of adrenergic C1 neurons causes sleep state-dependent cardiorespiratory stimulation and arousal with sighs in rats. Am J Respir Crit Care Med 190:1301–1310.

Burke PG, Kanbar R, Viar KE, Stornetta RL, Guyenet PG (2015a) Selective optogenetic stimulation of the retrotrapezoid nucleus in sleeping rats activates breathing without changing blood pressure or causing arousal or sighs. J Appl Physiol 118:1491–1501.

Burke PG, Kanbar R, Basting TM, Hodges WM, Viar KE, Stornetta RL, Guyenet PG (2015b) State-dependent control of breathing by the retrotrapezoid nucleus. J Physiol 593:2909–2926.

Carter ME, Yizhar O, Chikahisa S, Nguyen H, Adamantidis A, Nishino S, Deisseroth K, de Lecea L (2010) Tuning arousal with optogenetic modulation of locus coeruleus neurons. Nat Neurosci 13:1526–1533.

Cechetto DF, Standaert DG, Saper CB (1985) Spinal and trigeminal dorsal horn projections to the parabrachial nucleus in the rat. J Comp Neurol 240:153–160.

Chamberlin NL, Mansour A, Watson SJ, Saper CB (1999) Localization of mu-opioid receptors on amygdaloid projection neurons in the parabrachial nucleus of the rat. Brain Res 827:198–204.

Cregg JM, Chu KA, Dick TE, Landmesser LT, Silver J (2017) Phasic inhibition as a mechanism for generation of rapid respiratory rhythms. Proc Natl Acad Sci USA 114:12815–12820.

de Britto AA, Moraes DJ (2017) Non-chemosensitive parafacial neurons simultaneously regulate active expiration and airway patency under hypercapnia in rats. J Physiol 595:2043–2064.

Del Negro CA, Funk GD, Feldman JL (2018) Breathing matters. Nat Rev Neurosci 19:351–367.

Flor KC, Barnett WH, Karlen-Amarante M, Molkov YI, Zoccal DB (2020) Inhibitory control of active expiration by the Bötzinger complex in rats. J Physiol. Advance online publication. Retrieved Jul 4, 2020. doi: 10.1113/JP280243.

Gleeson K, Zwillich CW, White DP (1990) The influence of increasing ventilatory effort on arousal from sleep. Am Rev Respir Dis 142:295–300.

Guyenet PG, Mulkey DK, Stornetta RL, Bayliss DA (2005) Regulation of ventral surface chemoreceptors by the central respiratory pattern generator. J Neurosci 25:8938–8947.

Guyenet PG, Stornetta RL, Bochorishvili G, Depuy SD, Burke PG, Abbott SB (2013) C1 neurons: the body's EMTs. Am J Physiol Regul Integr Comp Physiol 305:R187–R204.

Guyenet PG, Stornetta RL, Souza G, Abbott SB, Shi Y, Bayliss DA (2019) The retrotrapezoid nucleus: central chemoreceptor and regulator of breathing automaticity. Trends Neurosci 42:807–824.

Holloway BB, Stornetta RL, Bochorishvili G, Erisir A, Viar KE, Guyenet PG (2013) Monosynaptic glutamatergic activation of locus coeruleus and other lower brainstem noradrenergic neurons by the C1 cells in mice. J Neurosci 33:18792–18805.

Huckstepp RT, Cardoza KP, Henderson LE, Feldman JL (2015) Role of parafacial nuclei in control of breathing in adult rats. J Neurosci 35:1052–1067.

Huckstepp RT, Henderson LE, Cardoza KP, Feldman JL (2016) Interactions between respiratory oscillators in adult rats. eLife 5:e14203.

Hwang DY, Carlezon WA Jr, Isacson O, Kim KS (2001) A high-efficiency synthetic promoter that drives transgene expression selectively in noradrenergic neurons. Hum Gene Ther 12:1731–1740.

Iscoe S (1998) Control of abdominal muscles. Prog Neurobiol 56:433–506.

Jansen AS, Nguyen XV, Karpitskiy V, Mettenleiter TC, Loewy AD (1995) Central command neurons of the sympathetic nervous system: basis of the fight-or flight response. Science 270:644–646.

Kaur S, Saper CB (2019) Neural circuitry underlying waking up to hypercapnia. Front Neurosci 13:401.

Kaur S, Wang JL, Ferrari L, Thankachan S, Kroeger D, Venner A, Lazarus M, Wellman A, Arrigoni E, Fuller PM, Saper CB (2017) A genetically defined circuit for arousal from sleep during hypercapnia. Neuron 96:1153–1167.e1155.

Li P, Janczewski WA, Yackle K, Kam K, Pagliardini S, Krasnow MA, Feldman JL (2016) The peptidergic control circuit for sighing. Nature 530:293–297.

Li P, Li SB, Wang X, Phillips CD, Schwarz LA, Luo L, de Lecea L, Krasnow MA (2020) Brain circuit of claustrophobia-like behavior in mice identified by upstream tracing of sighing. Cell Rep 31:107779.

Malheiros-Lima MR, Takakura AC, Moreira TS (2017) Depletion of rostral ventrolateral medullary catecholaminergic neurons impairs the hypoxic ventilatory response in conscious rats. Neuroscience 351:1–14.

Malheiros-Lima MR, Silva JN, Souza FC, Takakura AC, Moreira TS (2020) C1 neurons are part of the circuitry that recruits active expiration in response to the activation of peripheral chemoreceptors. eLife 9:e52572.

Marina N, Abdala AP, Trapp S, Li A, Nattie EE, Hewinson J, Smith JC, Paton JF, Gourine AV (2010) Essential role of Phox2b-expressing ventrolateral brainstem neurons in the chemosensory control of inspiration and expiration. J Neurosci 30:12466–12473.

Miller AD (1987) Localization of motoneurons innervating individual abdominal muscles of the cat. J Comp Neurol 256:600–606.

Moreira TS, Takakura AC, Colombari E, West GH, Guyenet PG (2007) Inhibitory input from slowly adapting lung stretch receptors to retrotrapezoid nucleus chemoreceptors. J Physiol 580:285–300.

Pagliardini S, Janczewski WA, Tan W, Dickson CT, Deisseroth K, Feldman JL (2011) Active expiration induced by excitation of ventral medulla in adult anesthetized rats. J Neurosci 31:2895–2905.

Palmiter RD (2018) The parabrachial nucleus: CGRP neurons function as a general alarm. Trends Neurosci 41:280–293.

Paxinos G, Waston C (2014) The rat brain in stereotaxic coordinates, Ed 7. San Diego: Academic.

Pisanski A, Pagliardini S (2019) The parafacial respiratory group and the control of active expiration. Respir Physiol Neurobiol 265:153–160.

Pisanski A, Ding X, Koch NA, Pagliardini S (2020) Chemogenetic modulation of the parafacial respiratory group influences the recruitment of abdominal activity during REM sleep. Sleep 43:12.

Road JD, Ford TW, Kirkwood PA (2013) Connections between expiratory bulbospinal neurons and expiratory motoneurons in thoracic and upper lumbar segments of the spinal cord. J Neurophysiol 109:1837–1851.

Schindelin J, Arganda-Carreras I, Frise E, Kaynig V, Longair M, Pietzsch T, Preibisch S, Rueden C, Saalfeld S, Schmid B, Tinevez JY, White DJ, Hartenstein V, Eliceiri K, Tomancak P, Cardona A (2012) Fiji: an open-source platform for biological-image analysis. Nat Methods 9:676–682.

Shi Y, Stornetta RL, Stornetta DS, Onengut-Gumuscu S, Farber EA, Turner SD, Guyenet PG, Bayliss DA (2017) Neuromedin B expression defines the mouse retrotrapezoid nucleus. J Neurosci 37:11744–11757.

Silva JN, Tanabe FM, Moreira TS, Takakura AC (2016) Neuroanatomical and physiological evidence that the retrotrapezoid nucleus/parafacial region regulates expiration in adult rats. Respir Physiol Neurobiol 227:9–22.

Smith HR, Leibold NK, Rappoport DA, Ginapp CM, Purnell BS, Bode NM, Alberico SL, Kim YC, Audero E, Gross CT, Buchanan GF (2018) Dorsal raphe serotonin neurons mediate CO_2-induced arousal from sleep. J Neurosci 38:1915–1925.

Smith JC, Morrison DE, Ellenberger HH, Otto MR, Feldman JL (1989) Brainstem projections to the major respiratory neuron populations in the medulla of the cat. J Comp Neurol 281:69–96.

Smith JC, Abdala AP, Borgmann A, Rybak IA, Paton JF (2013) Brainstem respiratory networks: building blocks and microcircuits. Trends Neurosci 36:152–162.

Souza G, Kanbar R, Stornetta DS, Abbott SB, Stornetta RL, Guyenet PG (2018) Breathing regulation and blood gas homeostasis after near complete lesions of the retrotrapezoid nucleus in adult rats. J Physiol 596:2521–2545.

Souza G, Stornetta RL, Stornetta DS, Abbott SB, Guyenet PG (2019) Contribution of the retrotrapezoid nucleus and carotid bodies to hypercapnia- and hypoxia-induced arousal from sleep. J Neurosci 39:9725–9737.

Stornetta RL, Moreira TS, Takakura AC, Kang BJ, Chang DA, West GH, Brunet JF, Mulkey DK, Bayliss DA, Guyenet PG (2006) Expression of phox2b by brainstem neurons involved in chemosensory integration in the adult rat. J Neurosci 26:10305–10314.

Viemari JC, Garcia AJ 3rd, Doi A, Elsen G, Ramirez JM (2013) β-Noradrenergic receptor activation specifically modulates the generation of sighs in vivo and in vitro. Front Neural Circuits 7:179.

Wakai J, Takamura D, Morinaga R, Nakamuta N, Yamamoto Y (2015) Differences in respiratory changes and Fos expression in the ventrolateral medulla of rats exposed to hypoxia, hypercapnia, and hypercapnic hypoxia. Respir Physiol Neurobiol 215:64–72.

Yang CF, Chiang MC, Gray DC, Prabhakaran M, Alvarado M, Juntti SA, Unger EK, Wells JA, Shah NM (2013) Sexually dimorphic neurons in the ventromedial hypothalamus govern mating in both sexes and aggression in males. Cell 153:896–909.